

# Structural Criteria for the Rational Design of Selective Ligands. 3. Quantitative Structure–Stability Relationship for Iron(III) Complexation by Tris-Catecholamide Siderophores

Benjamin P. Hay,<sup>\*,†</sup> David A. Dixon,<sup>†</sup> Rubicelia Vargas,<sup>‡</sup> Jorge Garza,<sup>‡</sup> and Kenneth N. Raymond<sup>§</sup>

Environmental Molecular Sciences Laboratory, Pacific Northwest National Laboratory, P.O. Box 999, Richland, Washington 99352, Departamento de Química, División de Ciencias Básicas e Ingeniería, Universidad Autónoma Metropolitana-Iztapalapa. A.P. 55-534, México Distrito Federal 09340, Mexico, and Department of Chemistry, University of California, Berkeley, California 94720

Received December 7, 2000

We present an extended MM3 model for catecholamide ligands and their Fe<sup>3+</sup> complexes and the application of this model to understand how ligand architecture effects Fe<sup>3+</sup> binding affinity. Force field parameters were fit to geometries and energies from electronic structure calculations, and to crystal structure data. Optimized geometries are reported for phenol, acetamide, the phenol–phenol dimer, the acetamide–phenol dimer, and *N*-methylsali-cylamide (HMSA) at the BLYP/DZVP2/A2 level of theory. Optimized geometries and relative energies are reported for the pseudo-octahedral ground state and the trigonal planar transition state of [Fe(CAT)<sub>3</sub>]<sup>3-</sup> at the VWN/DZVP2/A1 level of theory. The MM3 model is validated by comparison of calculated structures with crystal structures containing 1,2-dihydroxybenzene (H<sub>2</sub>CAT) and 2,3-dihydroxy-*N*-methylbenzamide (H<sub>2</sub>MBA) fragments, crystal structures of [Fe(CAT)<sub>3</sub>]<sup>3-</sup> and tris-catecholamide Fe<sup>3+</sup> complexes, and comparison of MM3 (6.8 kcal/mol) and VWN (5.9 kcal/mol) barriers for intramolecular octahedral inversion in [Fe(CAT)<sub>3</sub>]<sup>3-</sup>. The MM3 model also rationalizes the higher inversion barrier (14 to 18 kcal/mol) reported for [Ga(*N,N*-diisopropylterephthalamide)<sub>3</sub>]<sup>3-</sup> ([Ga(DIPTA)<sub>3</sub>]<sup>3-</sup>). Conformational searches were performed on enterobactin (H<sub>6</sub>ENT), 1,3,5-tris(2,3-dihydroxybenzamidomethyl)-2,4,6-triethylbenzene (H<sub>6</sub>EMECAM), 1,3,5-tris(2,3-dihydroxybenzamidomethyl)-2,4,6-trimethylbenzene (H<sub>6</sub>MMECAM), 1,3,5-tris(2,3-dihydroxybenzamidomethyl)benzene (H<sub>6</sub>MECAM), and 1,5,9-*N,N',N''*-tris(2,3-dihydroxybenzoyl)cyclotriazatridecane (H<sub>6</sub>-3,3,4-CYCAM) and Fe<sup>3+</sup> complexes with each of these ligands. A conformational search also was done on the Fe<sup>3+</sup> complex with the 2,2',2''-tris(2,3-dihydroxybenzamido)-triethylammonium cation (H<sub>7</sub>TRENCAM<sup>+</sup>). The relationship between calculated steric energies and measured thermodynamic quantities is discussed, and linear correlations between formation constants and steric energy differences are reported. Extrapolation to zero strain predicts formation constants 8 ± 5 orders of magnitude higher than that exhibited by ENT (10<sup>49</sup>) are possible. This prediction is supported by a formation constant of 10<sup>63</sup> estimated from the formation constant of [Fe(2,3-dihydroxy-*N,N*-dimethylbenzamide)<sub>3</sub>]<sup>3-</sup> ([Fe(DMBA)<sub>3</sub>]<sup>3-</sup>) by considering the entropic consequences of connecting three DMBA ligands to a rigid backbone. Structural criteria for the identification of improved tris-catecholate ligand architectures are presented.

## Introduction

A critical aspect of the deliberate design of selective metal ion hosts is the selection of connecting or backbone structure that provides optimal positioning of donor groups for the targeted metal ion. The effort to increase selectivity of the host for one metal over another is the selection of architecture that provides an optimal positioning of donor groups for that metal only, and that does not allow structural reorganization of the host to accommodate other metals.<sup>1</sup> A large number of possible architectures exist for any given set of donor groups, but only a limited number of architectures can be examined by experiment. As a result, it is often possible to conceive many more structures than it is possible to prepare, and the chemist must then apply some criteria to select candidates for subsequent synthesis. The critical path to success requires an accurate set

of criteria to predict how host architecture will influence metal ion complexation.

It has long been recognized that increased binding affinities are obtained when a collection of donor atoms is structurally constrained to a binding conformation. This observation, which is embodied in the concepts of multi-juxtapositional fixedness,<sup>2</sup> prestraining,<sup>3</sup> preorienting,<sup>4</sup> preorganization,<sup>5</sup> and predisposition,<sup>6</sup> provides two caveats for the design of effective complexants: (i) multidentate ligands are preferred over groups of unidentate ligands and (ii) rigid ligands are preferred over

<sup>†</sup> Pacific Northwest National Laboratory.

<sup>‡</sup> Universidad Autónoma Metropolitana-Iztapalapa. A.P. 55-534.

<sup>§</sup> University of California.

(1) Hancock, R. D.; Martell, A. E. *Chem. Rev.* **1989**, 89, 1875.

(2) Busch, D. H.; Farmery, K.; Goedken, V.; Katovic, V.; Melnyk, A. C.; Sperati, C. R.; Tokel, N. *Adv. Chem. Ser.* **1971**, 100, 44.

(3) McDougall, G. J.; Hancock, R. D.; Boeyens, J. C. A. *J. Chem. Soc., Dalton Trans.* **1978**, 1438.

(4) Anicini, A.; Fabbizzi, L.; Paoletti, P.; Clay, R. M. *J. Chem. Soc., Dalton Trans.* **1978**, 577.

(5) Cram, D. J.; Kaneda, T.; Helgeson, R. C.; Brown, S. B.; Knobler, C. B.; Maverick, E.; Trueblood, K. N. *J. Am. Chem. Soc.* **1985**, 107, 3645.

(6) Stack, T. D. P.; Hou, Z.; Raymond, K. N. *J. Am. Chem. Soc.* **1993**, 115, 6466.

flexible ligands. Conformational flexibility can result in quite different cavity sizes and shapes. Consequently, different conformers may exhibit different metal ion selectivities. The first prerequisite for predicting the influence of ligand architecture on metal ion complexation is the identification of the stable conformations of the ligand and its metal complexes.

Once the binding conformation(s) of a ligand is(are) identified, the remaining issue is the degree of structural correspondence between the binding sites offered by the ligand and the binding sites required by the metal; that is, how well does the ligand architecture complement the metal.<sup>7,8</sup> While many practitioners limit discussion of complementarity to a comparison of the size of the ligand cavity with the radius of the metal ion, a complete analysis of complementarity requires a consideration of M–L distances as well as donor group orientation (M–L–X and M–L–X–X angles) and, in some cases, the topography of the metal ion (L–M–L angles) where M = metal, L = donor atom, and X = any other atom.<sup>9</sup> Failure to provide one or more of these geometric features can lead to significant decreases in binding affinity. A second prerequisite for predicting the influence of ligand architecture on metal ion complexation is the identification of the geometric features that are required to achieve the most stable interactions between the metal ion and the binding sites.

With increasing application to coordination compounds,<sup>9–18</sup> molecular mechanics (MM) models provide an ideal, computationally efficient tool to evaluate the degree to which a ligand is structurally organized for metal complexation.<sup>9,19–22</sup> Conformational analyses yield the stable conformers of the ligand both in the uncomplexed state and in the metal complex. MM models partition the steric energy into stretching, bending, torsion, and nonbonded (e.g., van der Waals, electrostatics, hydrogen bonding) interactions. The process of parametrizing these models requires knowledge of the geometries and potential energy surfaces for each individual interaction, which are precisely the criteria needed to evaluate metal ion complementarity. Examination of the steric energy components from calculations on metal

ion complexes provides a way to quantify the effect of (i) cavity size mismatch (strain in M–L bonds), (ii) poor donor group orientation (strain in M–L–X and M–L–X–X angles), and (iii) topographical mismatch (strain in L–M–L angles).<sup>9</sup>

In prior papers of this series, MM models were parametrized to provide a basis for the evaluation of complementarity in polyether complexes with alkali and alkaline earth cations,<sup>21</sup> and a method was developed for using MM strain energies as a measurement of the degree of binding site organization offered by a ligand architecture.<sup>22</sup> This approach provides a framework for rationalizing the effect of architectural variation on binding affinity in series of ligands bearing the same number and type of binding sites. Its application has yielded a number of quantitative structure stability relationships which demonstrate that the steric strain in isolated ligands and metal complexes, that is, calculated in the absence of solvent, can be used successfully to correlate condensed phase binding affinities.<sup>19–26</sup> The current paper describes the development and application of these methods to another system, the Fe<sup>3+</sup> complexes of tris-catecholamides.

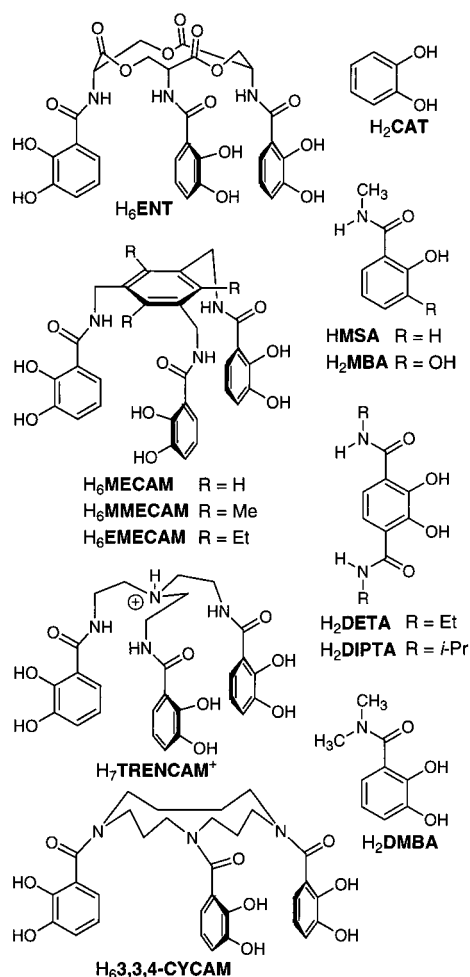
The tris-catecholamides H<sub>6</sub>ENT, H<sub>6</sub>MECAM, H<sub>6</sub>MMECAM, H<sub>6</sub>EMECAM, H<sub>7</sub>TRENCAM<sup>+</sup>, and H<sub>6</sub>3,3,4-CYCAM (Figure 1) are a series of ligands that contain a constant set of donor groups connected to different backbones. Thermodynamic studies have established that this variation of ligand architecture yields Fe<sup>3+</sup> binding constants that span a range of 9 orders-of-magnitude.<sup>27–30</sup> Herein we examine whether it is possible to rationalize this behavior through the analysis of MM strain energies. We report the development and validation of an extended MM model for catecholamides and their Fe<sup>3+</sup> complexes, and the application of this model to evaluate the degree of binding site organization in the tris-catecholamides shown in Figure 1.

## Theoretical Methods

**Molecular Mechanics Calculations.** Molecular mechanics calculations were performed with the MM3(96) program.<sup>31</sup> The Fe(III) metal ion was designated as a “points-on-a-sphere” (POS) center;<sup>15,32</sup> in other words, interactions involving this atom type were limited to Fe–O stretches, Fe–O–C bends, and Fe–O–C–C torsions. The O–Fe–O angles were dictated by nonbonded interactions between the inner-

- (7) (a) Cram, D. J.; Lein, G. M. *J. Am. Chem. Soc.* **1985**, *107*, 3657. (b) Cram, D. J. *Angew. Chem., Int. Ed. Engl.* **1986**, *25*, 1039.
- (8) (a) Busch, D. H. *Chem. Rev.* **1993**, *93*, 847. (b) Busch, D. H. *Transition Metals in Supramolecular Chemistry*; Fabbrizzi, L.; Poggi, A., Eds.; Kluwer Academic Publishers: Netherlands, 1994; pp 55–80.
- (9) Hay, B. P.; Hancock, R. D. *Coord. Chem. Rev.* **2001**, *212*, 61.
- (10) Brubaker, G. R.; Johnson, D. W. *Coord. Chem. Rev.* **1984**, *53*, 1.
- (11) Hancock, R. D. *Progr. Inorg. Chem.* **1989**, *37*, 188.
- (12) Pozigun, D. V.; Kuz'min, V. E.; Kamalov, G. L. *Russ. Chem. Rev.* **1990**, *59*, 1093.
- (13) Timofeeva, T. V.; Struchkov, Y. T. *Russ. Chem. Rev.* **1990**, *59*, 320.
- (14) (a) Comba, P. *Coord. Chem. Rev.* **1993**, *123*, 1. (b) Comba, P.; Hambley, T. W. *Molecular Modeling of Inorganic Compounds*; VCH: New York, 1995. (c) Comba, P. *Coord. Chem. Rev.* **1999**, *182*, 343. (d) Comba, P. *Coord. Chem. Rev.* **1999**, *185–186*, 81.
- (15) (a) Hay, B. P. *Coord. Chem. Rev.* **1993**, *126*, 177. (b) Hay, B. P.; Clement, O. In *The Encyclopedia of Computational Chemistry*; Schleyer, P. v. R.; Allinger, N. L.; Clark, T.; Gasteiger, J.; Kollman, P. A.; Schaefer, H. F., III.; Schreiner, P. R., Eds.; John Wiley & Sons: Chichester, 1998; pp 1580–1587.
- (16) Landis, C. R.; Root, D. M.; Cleveland, T. *Reviews in Computational Chemistry*; Lipkowitz, K. B.; Boyd, D. B., Eds.; VCH Publishers: New York, 1995; Vol. VI, pp 73–148.
- (17) Zimmer, M. *Chem. Rev.* **1995**, *95*, 2629.
- (18) Cundari, T. R. *J. Chem. Soc., Dalton Trans.* **1998**, 2771.
- (19) Hay, B. P. In *Metal-Ion Separation and Preconcentration, Progress and Opportunities*, ACS Symposium Series 716; Bond, A. H.; Dietz, M. L.; Rogers, R. D., Eds.; American Chemical Society: Washington, D. C., 1999; pp 102–113.
- (20) Hay, B. P. In *Metal Separation Technologies Beyond 2000: Integrating Novel Chemistry with Processing*; Liddell, K. C.; Chaiko, D. J., Eds.; Minerals, Metals, Materials Society: Warrendale, PA, 1999; pp 3–13.
- (21) Hay, B. P.; Rustad, J. R. *J. Am. Chem. Soc.* **1994**, *116*, 6316.
- (22) Hay, B. P.; Zhang, D.; Rustad, J. R. *Inorg. Chem.* **1996**, *35*, 2650.

- (23) Hay, B. P.; Rustad, J. R. *Supramol. Chem.* **1996**, *6*, 383.
- (24) Hay, B. P.; Rustad, J. R.; Hostetler, C. J. *J. Am. Chem. Soc.* **1993**, *115*, 11158.
- (25) Sachleben, R. A.; Moyer, B. A. In *Metal-Ion Separation and Preconcentration, Progress and Opportunities*, ACS Symposium Series 716; Bond, M. L.; Rogers, R. D., Ed.; American Chemical Society: Washington, DC, 1999; pp 114–132.
- (26) (a) Bond, A. H.; Chiarizia, R.; Huber, V. J.; Dietz, M. L.; Herlinger, A. W.; Hay, B. P. *Anal. Chem.* **1999**, *71*, 2757. (b) Dietz, M. L.; Bond, A. H.; Hay, B. P.; Chiarizia, R.; Huber, V. J.; Herlinger, A. W. *Chem. Commun.* **1999**, *13*, 1177.
- (27) (a) Harris, W. R.; Carrano, C. J.; Cooper, S. R.; Sofen, S. R.; Avdeef, A.; McArdle, J. V.; Raymond, K. N. *J. Am. Chem. Soc.* **1979**, *101*, 6097. (b) Loomis, L. D.; Raymond, K. N. *Inorg. Chem.* **1991**, *30*, 906.
- (28) Harris, W. R.; Raymond, K. N. *J. Am. Chem. Soc.* **1979**, *101*, 6534.
- (29) Hou, Z.; Stack, T. D. P.; Sunderland, C. J.; Raymond, K. N. *Inorg. Chim. Acta* **1997**, *263*, 341.
- (30) Rodgers, S. J.; Lee, C.-W.; Ng, C. Y.; Raymond, K. N. *Inorg. Chem.* **1987**, *26*, 1622.
- (31) MM3(96). The program may be obtained from Tripos Associates, 1699 S. Hanley Road, St. Louis, MO 63144 for commercial users, and it may be obtained from the Quantum Chemistry Program Exchange, Mr. Richard Counts, QCPE, Indiana University, Bloomington, IN 47405, for noncommercial users.
- (32) For early applications of the POS method, see: (a) Niketic, S. R.; Woldbye, F. *Acta Chem. Scand.* **1973**, *27*, 621. (b) Hambley, T. W.; Hawkins, C. J.; Palmer, J. A.; Snow, M. R. *Aust. J. Chem.* **1981**, *34*, 45.



**Figure 1.** Structures of the ligands discussed in this study.

sphere oxygen atoms. In our application of the POS model,<sup>33</sup> all nonbonded interactions that involve Fe<sup>3+</sup> are assumed to be implicitly treated in the stretching, bending, and torsional interactions. Therefore, van der Waals and electrostatic interactions involving Fe<sup>3+</sup> were intentionally excluded from the calculation by setting the corresponding parameters to zero. In addition, we assumed that there is a negligible intrinsic barrier to Fe–O bond rotation and all O–Fe–O–C torsional interactions were excluded from the calculation. Energy minimizations were done with the block diagonal Newton–Raphson method followed by the full-matrix Newton–Raphson method using a convergence criterion of rms force of 0.0001 kcal mol<sup>−1</sup> Å<sup>−1</sup>.

It is necessary to modify the default MM3 force field to allow application to catecholamide ligands and their Fe<sup>3+</sup> complexes. One modification has to do with the treatment of extended  $\pi$ -systems in the MM3 model. In normal operation, MM3 employs a VESCF calculation to determine the bond orders for the  $\pi$ -system bonds and assigns stretching and torsional force constants based on these bond orders.<sup>34</sup> Because the parameters needed to perform these calculations are not available for the substituents present in catecholamides, we did not use this feature of the model. Instead, we reassigned all C(arene)–C(arene) stretch and X–C(arene)–C(arene)–X torsion (X = any atom type) parameters to be the same as those assigned to benzene.

A second modification had to do with amide parameters. The default stretching and torsional parameters pertaining to the amide functional group were treated as described in our previous reports on modeling

aliphatic amides<sup>35</sup> and metal amide complexes.<sup>33b</sup> The default MM3 parameter set does not include bending and torsional interactions needed to model the benzamide functional group found in all catecholamides. The missing parameters, previously assigned by fitting to the MP2/aug-cc-pVTZ//BLYP/DZVP2/A2 potential energy surface for C(sp<sup>2</sup>)–C(aryl) rotation in *N*-methylbenzamide,<sup>36</sup> were added to the parameter set. In addition, the default MM3 parameter set does not include bending and torsional interactions needed to model the *N*-benzylamide functional group found in H<sub>6</sub>MECAM, H<sub>6</sub>MMECAM, and H<sub>6</sub>EMECAM. The missing parameters, previously assigned by fitting to the MP2/aug-cc-pVTZ//BLYP/DZVP2/A2 potential energy surfaces for rotation about N(amide)–C(sp<sup>3</sup>) and C(sp<sup>3</sup>)–C(aryl) bonds in *N*-benzylformamide,<sup>37</sup> were added to the parameter set.

The above modifications were required to obtain an MM3 model that would accept a catecholamide input structure, that is, all bonded interactions were represented in the parameter set. Further parametrization, however, was needed to include the various types of hydrogen bonds found in this class of ligands. These parameters were assigned by fitting to geometries and interaction energies obtained from electronic structure calculations (vide infra) on the phenol dimer, the phenol–acetamide dimer, and HMB. Experimental data on H<sub>2</sub>CAT and catecholamide geometries, obtained by analysis of crystal structures from the Cambridge Structural Database (CSD),<sup>38</sup> were used to check the performance of the model.

The MM3 parameter set was modified further to model Fe<sup>3+</sup> complexes with this class of ligands. The strain-free length for the C(arene)–O bond was shortened by 0.03 Å after comparison of H<sub>2</sub>CAT and metal–CAT geometries. The default van der Waals radius of the catecholate oxygen was increased by 16% to account for an increase in size expected on going from neutral oxygen to anionic oxygen.<sup>39</sup> Finally, three Fe<sup>3+</sup> dependent interactions, Fe–O stretch, Fe–O–C bend, and Fe–O–C–C torsion, were parametrized by fitting to crystal structure data and potential energy surfaces from electronic structure calculations on [Fe(CAT)<sub>3</sub>]<sup>3−</sup> (vide infra). The performance of the model was validated by the ability to reproduce experimental structures taken from the CSD and the barrier to octahedral inversion in [Fe(CAT)<sub>3</sub>]<sup>3−</sup>.

MM3 parameter input files containing all changes to the default parameter set are provided as Supporting Information.

**Conformational Analyses.** Using the modified MM3 model described above, conformational searches were performed on the Fe<sup>3+</sup> complexes of ENT, EMECAM, MMECAM, MECAM, TRENCAM, and 3,3,4-CYCAM, and on the metal-free ligands H<sub>6</sub>ENT, H<sub>6</sub>EMECAM, H<sub>6</sub>MMECAM, H<sub>6</sub>MECAM, and H<sub>3,3,4</sub>-CYCAM. The searches were done using the Saunders' stochastic search algorithm<sup>40</sup> that is present as a subroutine in the MM3 program. In this method, the atomic coordinates of the input structure are randomly displaced and the resulting structure is optimized and stored. Successive iterations involve selecting a structure from the stored list, randomizing the coordinates, optimization, and storing the result. Searches were run for 5000 iterations with each protonated ligand and 500 iterations with each Fe<sup>3+</sup> complex. The absence of imaginary frequencies confirmed all low energy structures to be minima on the MM3 potential surface. MM3 input files for the minimum energy structures of each ligand and Fe<sup>3+</sup> complex are provided as Supporting Information.

**Electronic Structure Calculations.** Geometries of phenol, acetamide, the phenol dimer, the phenol–acetamide dimer, and HMSA

(33) (a) Hay, B. P.; Yang, L.; Allinger, N. L.; Lii, J.-H. *J. Mol. Struct. (THEOCHEM)* **1998**, 428, 203. (b) Hay, B. P.; Clement, O.; Sandrone, G.; Dixon, D. A. *Inorg. Chem.* **1998**, 37, 5887.

(34) (a) Allinger, N. L.; Li, F.; Yan, L. *J. Comput. Chem.* **1990**, 11, 848. (b) Allinger, N. L.; Li, F.; Yan, L.; Tai, J. C. *J. Comput. Chem.* **1990**, 11, 868.

(35) Sandrone, G.; Dixon, D. A.; Hay, B. P. *J. Phys. Chem. A* **1999**, 103, 993.

(36) Vargas, R.; Garza, J.; Dixon, D. A.; Hay, B. P. *J. Phys. Chem. A* **2001**, 105, 774.

(37) Vargas, R.; Garza, J.; Dixon, D. A.; Hay, B. P. *J. Mol. Struct. (THEOCHEM)* **2001**, 541, 243.

(38) *Cambridge Structural Database System, Version V5.18, October 1999 Release*; Allen, F. H.; Bellard, S. A.; Brice, B. A.; Cartwright, A.; Doubleday, A.; Higgs, H.; Hummelink, T.; Hummelink-Peters, B. G.; Kennard, O.; Motherwell, W. D. S.; Rodgers, J. R.; Watson, D. G. *Acta Crystallogr., Sect. B* **1979**, 35, 2331.

(39) Ujaque, G.; Maseras, F.; Eisenstein, O. *Theor. Chem. Acc.* **1997**, 96, 146.

(40) Saunders, M. J. *Am. Chem. Soc.* **1987**, 109, 3150.



were optimized using density functional theory (DFT).<sup>41</sup> Although DFT at the local level fails to reproduce the structure and energetics of hydrogen bonded systems, gradient-corrected DFT can be used to predict moderate to strong hydrogen bonding interactions yielding good geometries and interaction energies to within 1 to 2 kcal/mol.<sup>42</sup> The DFT calculations were done with the DGAUSS program system<sup>43</sup> using the generalized gradient approximation (BLYP exchange-correlation functional)<sup>44</sup> and a polarized double- $\zeta$  basis set (DZVP2) in conjunction with the A2 fitting basis set.<sup>45</sup> Frequencies were calculated analytically. The absence of imaginary (negative) frequencies confirmed all structures to be minima. Single point energy calculations at the BLYP/DZVP2/A2 geometries were carried out with the NWChem program<sup>46</sup> at the second-order Møller–Plesset Perturbation (MP2)<sup>47</sup> level of theory using the aug-cc-pVTZ basis set.<sup>48</sup>

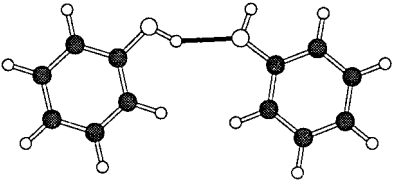
Geometries for the pseudo-octahedral ground state and the trigonal prismatic transition state of  $[\text{Fe}(\text{CAT})_3]^{3-}$  were optimized using DFT with the DGAUSS program system using the local density approximation (VWN exchange-correlation functional)<sup>49</sup> and a polarized double- $\zeta$  basis set (DZVP2) in conjunction with the A1 fitting basis set.<sup>45</sup> The structures were characterized by computing second derivatives to confirm that the ground-state structure was a minimum (no negative frequencies) and the transition state structure was a maximum (single negative frequency). Two potential energy surfaces for structural distortion of  $[\text{Fe}(\text{CAT})_3]^{3-}$  were generated by constraining selected structural features while fully optimizing the rest of the structure. The six Fe–O distances were constrained to 1.93, 1.98, 2.03, and 2.13 Å to yield a potential energy surface for distortion of Fe–O bonds. The six initially eclipsed Fe–O–C dihedral angles were constrained to 0, 5, 15, and 25° to yield a potential energy surface for an out-of-plane distortion of the chelate rings.

Geometries and energies obtained from the electronic structure calculations are provided as Supporting Information.

## Results and Discussion

**Model Parametrization and Validation for Catecholamide Ligands. (a) Hydrogen Bonding in  $\text{H}_2\text{CAT}$ .** A search of the CSD yielded 95 structural fragments that contain 1,2-dihydroxybenzene with H atoms in the 3 and 6 positions and either C or H atoms in the 4 and 5 positions. The majority of these structures exhibit an intramolecular hydrogen bond in which one of the hydroxyl groups is a donor and the other is an acceptor. The geometry and interaction energy of this type of hydrogen bond were investigated with electronic structure calculations on the phenol dimer. The results are summarized in Table 1. MM3 parameters of  $r^* = 2.023$  Å and  $\epsilon^* = 6.070$

**Table 1.** Hydrogen Bonding in the Phenol Dimer<sup>a</sup>



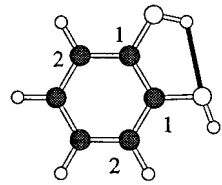
feature	BLYP	MM3
O...H	1.96	1.96
O...O	2.84	2.88
O–H...O	148	160
C–O...H	149	140
$\Delta E$ (BLYP) <sup>b</sup>	–4.2	
$\Delta E$ (MP2) <sup>c</sup>	–6.7	–6.7

<sup>a</sup> Units: distance (Å), angle (deg), energy (kcal/mol). Geometries optimized at the BLYP DZVP2/A2 level of theory and using MM3.

<sup>b</sup>  $E(\text{phenol dimer}) - 2E(\text{phenol})$  using BLYP/DZVP2/A2 energies.

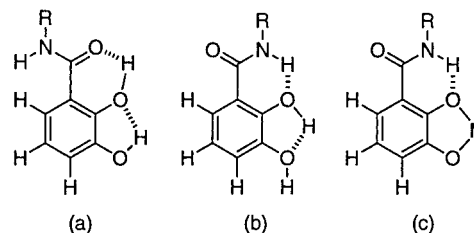
<sup>c</sup>  $E(\text{phenol dimer}) - 2E(\text{phenol})$  using single point MP2/aug-cc-pVTZ energies at the BLYP/DZVP2/A2 geometries.

**Table 2.** Comparison of Experimental and MM3 Structural Features for  $\text{H}_2\text{CAT}$ <sup>a</sup>



feature	exp	MM3
C–C	1.40(1)	1.398
C–O	1.37(1)	1.372
O...O	2.69(7)	2.725
O–C–C <sub>1</sub>	118(3)	118.8
O–C–C <sub>2</sub>	122(3)	121.2

<sup>a</sup> Units: distance (Å), angle (deg). Experimental values are averaged over 95 structural fragments. Standard deviations are given in parentheses.



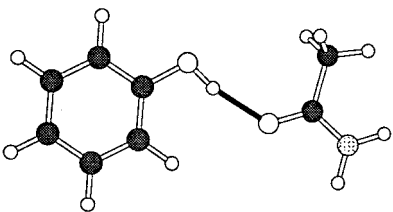
**Figure 2.** Hydrogen bonding motifs for the catecholamide ligand.

kcal/mol were assigned to this hydrogen bond by fitting to the O...H distance and the MP2 interaction energy. For comparison, the MM3 parameters for a hydrogen bond between aliphatic alcohol donor and acceptor, such as the methanol dimer, at  $r^* = 2.110$  Å and  $\epsilon^* = 3.00$  kcal/mol.<sup>50</sup> The stronger interaction in the case of phenol can be rationalized in terms of the higher acidity of the phenol hydrogen. The results presented in Table 2 establish that the MM3 model reproduces the observed structural parameters of the  $\text{H}_2\text{CAT}$  moiety to within experimental deviations.

**(b) Hydrogen Bonding in DHMB.** Catecholamides have two possible hydrogen bonding motifs (Figure 2a and 2b). In the first motif, the *meta* O–H binds to the *ortho* oxygen atom and the *ortho* O–H bonds to the amide oxygen atom. Alternatively,

- (41) Parr, R. G.; Yang, W. *Density-Functional Theory of Atoms and Molecules*; Oxford University Press: New York, 1989.
- (42) Vargas, R.; Garza, J.; Dixon, D. A.; Hay, B. P. Unpublished results.
- (43) DGAUSS is a density functional program, which is part of Unichem and is available from Oxford Molecular. (a) Andzelm, J.; Wimmer, E.; Salahub, D. R. In *The Challenge of d and f Electrons: Theory and Computation*; Salahub, D. R., Zerner, M. C., Eds.; ACS Symposium Series 394; American Chemical Society: Washington, DC, 1989; p 228. (b) Andzelm, J. In *Density Functional Theory in Chemistry*; Labanowski, J., Andzelm, J., Eds.; Springer-Verlag: New York, 1991; p 155. (c) Andzelm, J. W.; Wimmer, E. *J. Chem. Phys.* **1992**, 96, 1280.
- (44) (a) Becke, A. D. *Phys. Rev. A* **1988**, 38, 3098. (b) Lee, C.; Yang, W.; Parr, R. G. *Phys. Rev. B* **1988**, 37, 785.
- (45) Godbout, N.; Salahub, D. R.; Andzelm, J.; Wimmer, E. *Can. J. Chem.* **1992**, 70, 560.
- (46) Bernholdt, D. E.; Apra, E.; Fruchtl, H. A.; Guest, M. F.; Harrison, R. J.; Kendall, R. A.; Kutteh, R. A.; Long, X.; Nicholas, J. B.; Nichols, J. A.; Taylor, H. L.; Wong, A. T.; Fann, G. I.; Littlefield, R. J.; Nieplocha, J. *Int. J. Quantum Chem. Symp.* **1995**, 29, 475.
- (47) (a) Møller, C.; Plesset, M. S. *Phys. Rev.* **1934**, 46, 618. (b) Pople, J. A.; Binkley, J. S.; Seeger, R. *Int. J. Quantum Chem. Symp.* **1976**, 10, 1.
- (48) (a) Dunning, T. H., Jr. *J. Chem. Phys.* **1989**, 90, 1007. (b) Kendall, R. A.; Dunning, T. H., Jr.; Harrison, R. J. *J. Chem. Phys.* **1992**, 96, 6769.
- (49) Vosko, S. J.; Wilk, L.; Nusair, W. *Can. J. Phys.* **1980**, 58, 1200.

(50) Lii, J.-H.; Allinger, N. L. *J. Phys. Org. Chem.* **1994**, 7, 591.

**Table 3.** Hydrogen Bonding in the Phenol–Acetamide Dimer<sup>a</sup>


feature	BLYP	MM3
O - - H	1.77	1.77
O - - O	2.77	2.73
O–H - - O	176	175
C–O - - H	123	131
$\Delta E$ (BLYP) <sup>b</sup>	–9.9	
$\Delta E$ (MP2) <sup>c</sup>	–12.0	–12.0

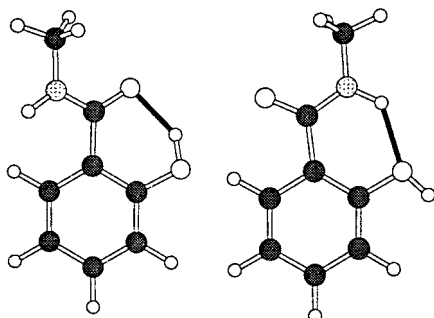
<sup>a</sup> Units: distance (Å), angle (deg), energy (kcal/mol). Geometries optimized at the BLYP/DZVP2/A2 level of theory and using MM3.  
<sup>b</sup>  $E(\text{phenol-acetamide dimer}) - E(\text{phenol}) - E(\text{acetamide})$  using BLYP/DZVP2/A2 energies.  
<sup>c</sup>  $E(\text{phenol-acetamide dimer}) - E(\text{phenol}) - E(\text{acetamide})$  using single point MP2/aug-cc-pVTZ energies at the BLYP/DZVP2/A2 geometries.

rotation about the C(sp<sup>2</sup>)–C(aryl) bond allows the amide N–H to bond to the *ortho* oxygen atom and *ortho* O–H bonds to the *meta* O–H oxygen atom. The first motif is observed in all crystal structures containing the 2,3-dihydroxy-*N*-alkylbenzamide moiety. When the catecholamide ligand is deprotonated, the form that is present in metal complexes, there is a single hydrogen bonding motif in which the amide N–H group bonds to the *ortho* oxygen atom (Figure 2c).

The geometry and interaction energy of the O–H - - O(amide) hydrogen bond was modeled with electronic structure calculations on the phenol–acetamide dimer. The results are summarized in Table 3. MM3 hydrogen bond parameters  $r^* = 1.847$  Å and  $\epsilon^* = 10.550$  kcal/mol were assigned by fitting to the O - - H distance and the MP2 dissociation energy. These parameters can be compared with the MM3 parameters of  $r^* = 2.07$  Å and  $\epsilon^* = 2.55$  kcal/mol for a hydrogen bond between an aliphatic alcohol donor and an amide carbonyl acceptor.<sup>51</sup> As in the comparison of the phenol dimer to aliphatic alcohols (vide supra), the difference is consistent with the higher acidity of the phenol hydrogen.

Electronic structure calculations were used to investigate the geometries and relative energy of the two hydrogen bonding motifs in the model compound HMSA. The results are summarized in Table 4. Consistent with crystal structure data, both BLYP and MP2 predict that the O–H - - O form is significantly more stable than the N–H - - O form. MM3 hydrogen bond parameters  $r^* = 2.170$  Å and  $\epsilon^* = 1.000$  kcal/mol were assigned to the N–H - - O hydrogen bond in HMSA by fitting to the N–H - - O distance and the difference in MP2 energy between the two forms. These parameters can be compared with the MM3 parameters of  $r^* = 2.03$  Å and  $\epsilon^* = 5.14$  kcal/mol for a hydrogen bond between an amide N–H donor and an aliphatic alcohol acceptor.<sup>51</sup> Here, the difference is consistent with the weaker basicity of the phenol oxygen acceptor.

In the O–H - - O form, rotation about the C(sp<sup>2</sup>)–C(aryl) bond results in a nonplanar structure due to unfavorable nonbonded interactions between the N–H and the *ortho* arene hydrogen atom. The BLYP model gives a 6° rotation whereas the MM3 model gives a 27° rotation. As a result, MM3 yields an O - - O distance that is 0.08 Å longer. Addition calculations

**Table 4.** Hydrogen Bonding in HMSA<sup>a</sup>


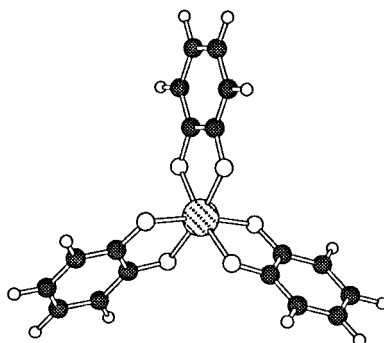
feature	BLYP	MM3
O–H - - O form		
O - - H	1.61	1.79
O - - O	2.56	2.64
O–H - - O	152	145
C–O - - H	102	98
O=C–C–C	6	27
N–H - - O form		
O - - H	1.93	1.94
N - - O	2.75	2.74
O–H - - O	135	132
C–O - - H	103	103
O=C–C–C	0	0
$\Delta E$ (BLYP) <sup>b</sup>	7.2	
$\Delta E$ (MP2) <sup>c</sup>	6.1	6.1

<sup>a</sup> Units: distance (Å), angle (deg), energy (kcal/mol). Geometries optimized at the BLYP/DZVP2/A2 level of theory and using MM3.  
<sup>b</sup>  $E(\text{N–H - - O form}) - E(\text{O–H - - O form})$  using BLYP/DZVP2/A2 energies.  
<sup>c</sup>  $E(\text{N–H - - O form}) - E(\text{O–H - - O form})$  using single point MP2/aug-cc-pVTZ energies at the BLYP/DZVP2/A2 geometries.

reveal that the MM3 rotational potential energy surface is relatively shallow and predict an energy penalty of only ~0.2 kcal/mol for rotation of  $\pm 10^\circ$  from the minimum and ~0.4 kcal/mol for rotation of  $\pm 20^\circ$ .

The N–H - - O hydrogen bond parameters given above are not transferable to the N–H - - O hydrogen bond found in deprotonated catecholamide chelates. A second set of N–H - - O parameters,  $r^* = 1.68$  Å and  $\epsilon^* = 10.0$  kcal/mol, were assigned by fitting to crystal structure data of complexed catecholamides. A search of the CSD yielded 24 structural fragments for deprotonated catecholamide chelates with *N*-alkyl substituents and H atoms in the 4, 5, and 6 positions. The structural features of these fragments were compared with those obtained by MM3 calculation on MBA in which the bite was fixed at 2.55 Å in order to mimic the average distance observed in metal complexes. The CSD also yielded six structural fragments that contain 2,3-dihydroxy-*N*-alkylbenzamide fragments with H atoms in the 4, 5, and 6 positions. The structural features in these fragments were with those obtained by MM3 calculation on H<sub>2</sub>MBA. In both cases, distances and bond angles are reproduced to within experimental deviations (a table of these comparisons is provided in the Supporting Information). Significant differences between the MM3 results and the X-ray data occurs with the degree of rotation about the about the C(sp<sup>2</sup>)–C(aryl) bond in the protonated molecule. As discussed earlier, these differences correspond to a relatively minor difference in energy.

**Model Parametrization and Validation for Fe<sup>3+</sup> Complexes.** (a) [Fe(CAT)<sub>3</sub>]<sup>3–</sup>. The structure of [Fe(CAT)<sub>3</sub>]<sup>3–</sup> was optimized at the VWN/DZVP2/A1 level of theory. The geometric features are presented in Table 5 where they are compared with the average observed geometry from two crystal structures

**Table 5.** Comparison of Experimental and Calculated Structural Features for the  $[\text{Fe}(\text{CAT})_3]^{3-}$  Complex<sup>a</sup>

	Fe—O	O—Fe—O	bite	O—O <sub>cap</sub>	Fe—O—C	Fe—O—C—C	twist angle
exp <sup>b</sup>	2.017(16)	81.2(6)	2.626(8)	2.88(5)	112.2(7)	4(3)	46(1)
VWN	2.034	79.5	2.603	2.913	114.0	0	43
MM3	2.017	81.0	2.622	2.909	112.2	0	48

<sup>a</sup> Units: distances (Å), angles (deg). The O—O distances within each chelate (bite) and within each cap of the octahedron (O—O<sub>cap</sub>) are given. The O—Fe—O value refers to the intrachelate angles only. The twist angle is defined in tris-chelate metal complexes as the angle between two coordinating atoms in the same chelate ring projected onto the plane perpendicular to the idealized 3-fold axis. <sup>b</sup> Averaged values taken from two crystal structures, BISCEL and KCATFE.<sup>52</sup> Standard deviations are given in parentheses.

that contain the  $[\text{Fe}(\text{CAT})_3]^{3-}$  complex.<sup>52</sup> Table 5 also shows the geometry obtained with MM3 after parametrization as described below.

The assignment of MM3 parameters for the  $\text{Fe}^{3+}$ -related interactions began with the Fe—O—C angle. Two parameters, the strain free angle,  $\theta_0$ , and the bending force constant,  $k_\theta$ , were assigned by fitting to the bite, in other words, the intrachelate O—O distance, observed in the experimental structures. The 2.63 Å bite in the coordinated catecholate ligand is, on average, shorter than the 2.69 Å value observed with catechol (Table 2). A similar decrease in bite on metal ion complexation is seen with catecholamide ligands. The bite decrease cannot be attributed to any intrinsic octahedral preference at the  $\text{Fe}^{3+}$  center because the intrachelate O—Fe—O angles are well below 90°.

An alternate hypothesis is that interchelate O—O repulsion accounts for the decreased bite. To test this hypothesis, a MM3 calculation was done in which the Fe—O distances were fixed at 2.017 Å with a large stretching force constant, the Fe—O—C—C dihedral angles were constrained to 0 or 180° with a large 2-fold rotational barrier, and the Fe—O—C bending interaction was omitted from the calculation by setting  $k_\theta = 0$ . This calculation gave a bite of 2.73 Å demonstrating that inter-chelate O—O repulsion, at least on the MM3 potential energy surface, does not explain the observed structure.

A final hypothesis, one that does account for the observed bite behavior, is that there is directional bonding at the coordinated oxygen atom center. In prior molecular mechanics studies of  $\text{Fe}^{3+}$  complexes, the Fe—O(phenolic)—C(sp<sup>2</sup>) bend interaction was assigned a “tetrahedral” preference<sup>53</sup> with parameters of  $\theta_0 = 107^\circ$  and  $k_\theta = 0.35 \text{ mdyne-Å/rad}^2$ , and a “trigonal planar” preference<sup>54</sup> with parameters of  $\theta_0 = 125^\circ$  and  $k_\theta = 0.42 \text{ mdyne-Å/rad}^2$ . Again holding Fe—O distance at 2.017 Å and the catecholates coplanar with the metal, application of these parameters to the  $[\text{Fe}(\text{CAT})_3]^{3-}$  complex yields bites

of 2.73 and 2.56 Å, respectively. Clearly, introducing a trigonal planar geometry at oxygen yields the correct behavior. The trigonal planar geometry is consistent with spectroscopic studies of the electronic structure of  $\text{Fe}^{3+}$  tris-catecholates which reveal both  $\sigma$  and  $\pi$  interactions to be present in Fe—O bonds.<sup>55</sup> In addition, trigonal planar oxygen is consistent with the 123 to 137° Fe—O—C angles observed in complexes that contain unidentate phenolate ligands in which the  $\text{Fe}^{3+}$  lies in the phenolate plane.<sup>56</sup> In the current application, we adopted the value of  $\theta_0 = 125^\circ$  cited above and assigned  $k_\theta = 0.184 \text{ mdyne-Å/rad}^2$  to reproduce the experimental bite of 2.63 Å.

After assignment of the Fe—O—C bend parameters, the Fe—O strain free length,  $r_0$ , and stretching force constant,  $k_r$ , were fit to a VWN potential energy surface by simultaneously varying all the Fe—O bond lengths in the  $[\text{Fe}(\text{CAT})_3]^{3-}$  complex. During the fitting process the Fe—O—C—C angles were constrained to planar values with a high 2-fold rotational barrier. The VWN energies were fit to within  $\pm 0.03 \text{ kcal/mol}$  to yield  $r_0 = 1.937 \text{ Å}$  and  $k_r = 2.024 \text{ mdyne-Å}^2$  (plot provided as Supporting Information). The  $r_0$  value was then adjusted to 1.931 Å to yield a model that gives the experimental Fe—O distance of 2.017 Å. The force constant obtained by this method is ~40% larger than the value of 1.43 mdyne-Å<sup>2</sup> predicted by Badger’s rule.<sup>57</sup> The parameters obtained here are significantly different from those reported in prior MM studies,  $r_0 = 1.995 \text{ Å}$  and  $k_r = 7.0 \text{ mdyne-Å}^2$ ,<sup>53</sup> and  $r_0 = 1.910 \text{ Å}$  and  $k_r = 0.76 \text{ mdyne-Å}^2$ .<sup>54</sup>

Finally, the 2-fold rotational barrier for the Fe—O—C—C torsion,  $V_2$ , was fit to a VWN potential energy surface for simultaneously distorting each arene ring out of the attached O—Fe—O planes. There is a significant energy increase when  $\text{Fe}^{3+}$  moves out of the catecholate plane, for example,  $\Delta E$  is 1.0 kcal/mol with an 8° deviation in Fe—O—C—C angle. This behavior provides further evidence for a trigonal planar geometry preference at the oxygen atoms. The VWN energies were

- (52) (a) KCATFE: Raymond, K. N.; Isied, S. S.; Brown, L. D.; Fronczek, F. R.; Nibert, J. H. *J. Am. Chem. Soc.* **1976**, *98*, 1767. (a) BISCEL: Anderson, B. F.; Buckingham, D. A.; Robertson, G. B.; Webb, J. *Acta Crystallogr., Sect. B* **1982**, *38*, 1927.  
(53) Zinelabidine, A.; Bouraoui, A.; Mhenni, F.; Blaive, B.; Gallo, R. J. *Mol. Struct. (THEOCHEM)* **1993**, *286*, 267.  
(54) Lin, W.; Welsh, W. J.; Harris, W. R. *Inorg. Chem.* **1994**, *33*, 884.

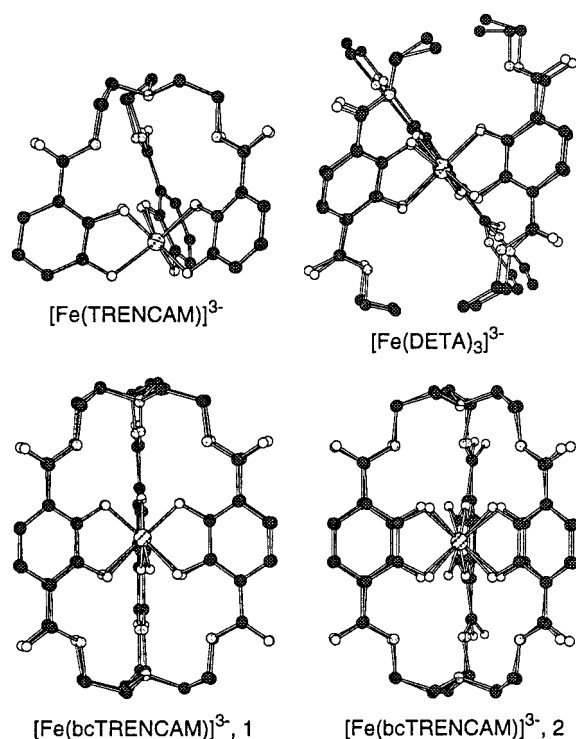
- (55) Karpishin, T. B.; Gebhard, M. S.; Solomon, E. I.; Raymond, K. N. *J. Am. Chem. Soc.* **1991**, *113*, 2977.  
(56) (a) CAPGAB: Cleland, W. E.; Holtman, D. A.; Sabat, M.; Ibers, J. A.; DeFotis, G. C.; Averill, B. A. *J. Am. Chem. Soc.* **1983**, *105*, 6021. (b) FEXBEP: Nasri, H.; Fischer, J.; Weiss, R.; Bill, E.; Trautwein, A. *J. Am. Chem. Soc.* **1987**, *109*, 2549.  
(57) (a) Badger, R. M. *J. Chem. Phys.* **1934**, *2*, 128. (b) Badger, R. M. *J. Chem. Phys.* **1935**, *3*, 710.



**Table 6.** Comparison of Experimental and Calculated Structures for Fe<sup>3+</sup> Tris-Catecholamide Complexes<sup>a</sup>

complex <sup>b</sup>		rmsd <sup>c</sup>	Fe—O	O—Fe—O <sup>d</sup>	bite <sup>d</sup>	Fe—O—C	Fe—O—C—C	twist angle <sup>d</sup>
JUTWEA	MM3	0.315	2.008	81.6	2.624	111.9	0	46.6
	exp <sup>58</sup>		2.029	79.0	2.585	114.2	5	40.0
SUCCUO	MM3	0.109	2.021	80.0	2.600	112.7	7	33.0
	exp <sup>59</sup>		2.009	79.5	2.570	113.0	12	37.4
JUTVOJ	MM3	0.201	2.003	79.9	2.572	113.7	0	2.7
	exp <sup>58</sup>		1.994	78.7	2.529	115.3	7	10.5
FUDRUR	MM3	0.308	2.004	79.9	2.572	113.6	3	0.0
	exp <sup>60</sup>		2.013	77.8	2.528	111.0	24	0.0
ave $\Delta$			$\pm 0.012$	$+1.6$	$+0.039$	$\pm 1.7$	$\pm 9$	$\pm 4.7$

<sup>a</sup> Units: Distances in Å, angles in degrees. <sup>b</sup> Cambridge Structural Database name. <sup>c</sup> Root-mean-squared deviation between the calculated and experimental positions for all non-hydrogen atoms. <sup>d</sup> See footnotes of Table 5 for definitions.

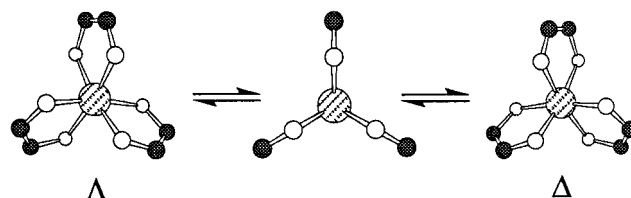
**Figure 3.** Overlays of experimental and calculated structures for tris-catecholamide Fe<sup>3+</sup> complexes.

fit to within  $\pm 0.01$  kcal/mol by adjusting  $V_2 = 1.859$  kcal/mol (plot provided as Supporting Information). This interaction was not parametrized in prior MM models for catecholates and phenolates.<sup>53,54</sup>

#### (b) Comparison of Experimental vs Calculated Structures.

Crystal structure data on four tris-catecholamide Fe<sup>3+</sup> complexes provide a benchmark to test the performance of the model. These complexes are [Fe(DETA)]<sup>3-</sup>,<sup>58</sup> [Fe(TRENCAM)]<sup>3-</sup>,<sup>59</sup> and two conformers of [Fe(bi-capped TRENCAM)]<sup>3-</sup>.<sup>58,60</sup> Starting from their crystal structure coordinates, these structures were calculated with the extended MM3 model. Figure 3 shows overlays of the calculated and experimental structures.

The root-mean-squared deviation (rmsd) between calculated and experimental atom positions for all non-hydrogen atoms, given in Table 6, range from 0.109 to 0.315 Å. The largest rmsd's occur in [Fe(DETA)]<sup>3-</sup> and the second [Fe(bi-capped TRENCAM)]<sup>3-</sup> structure. In the former structure, the Fe(CAT)<sub>3</sub>

**Figure 4.** The  $\Delta$  and  $\Lambda$  stereoisomers of a tris-chelate can interconvert through a trigonal prismatic transition state.

part of the complex is well reproduced, and the discrepancy is due primarily to the orientation of the *N*-ethyl substituents. In the latter structure, the crystal structure shows a large degree of out-of-plane distortion in the chelate rings which is not reproduced by the model. In both of these cases, the structural discrepancies are of the type that could be attributed to intermolecular forces present in the crystals.

Table 6 also provides a comparison of the average geometric features for the Fe(CAT)<sub>3</sub> component of the complexes. Experimental Fe—O distances, which range from 1.994 to 2.029 Å, are reproduced with an average deviation of  $\pm 0.012$  Å. In these complexes, the bites are overestimated by an average of 0.039 Å and, as a result, the O—Fe—O angles are overestimated by 1.6°. Experimental Fe—O—C angles, which range from 111.0 to 115.3°, are reproduced with an average deviation of  $\pm 1.7^\circ$ . Experimental Fe—O—C—C angles, which range from 5 to 24°, are underestimated on average by 9°. Finally, twist angles, which range from 0 to 40°, are reproduced with an average deviation of  $\pm 4.7^\circ$ .

**(c) Barriers to Octahedral Inversion in Tris-Chelates.** The barrier to octahedral inversion provides a further benchmark for validation of the model. As shown in Figure 4, tris-chelate complexes exhibit  $\Delta$  and  $\Lambda$  stereoisomers.<sup>61</sup> These enantiomers may interconvert via an intramolecular rearrangement which involves a concerted twist motion of the chelates about a trigonal face of the octahedron to generate a trigonal prismatic transition state.<sup>62</sup> The energetic barrier for inversion,  $\Delta E_{\text{inv}}$ , can be calculated as the difference in energy between the octahedral and trigonal prismatic forms of the complex. The VWN/DZVP2/A1 level of theory yields  $\Delta E_{\text{inv}} = 5.9$  kcal/mol for the [Fe(CAT)<sub>3</sub>]<sup>3-</sup> complex. The MM3 model yields  $\Delta E_{\text{inv}} = 6.8$  kcal/mol, reproducing the VWN value to within 1 kcal/mol.

The calculated  $\Delta E_{\text{inv}}$  value is consistent with activation enthalpies,  $\Delta H^\ddagger_{\text{inv}}$ , which have been measured for intramolecular octahedral inversion in the related tris-troponolate complexes. With this class of ligands, observed  $\Delta H^\ddagger_{\text{inv}}$  values range from 14 to 16 kcal/mol for Co<sup>3+</sup> and 10 to 12 kcal/mol

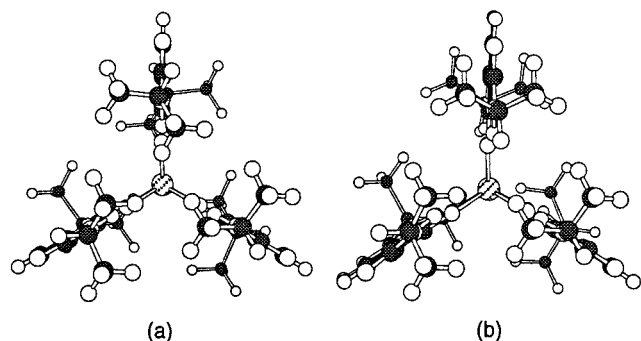
(58) JUTWEA and JUTVOJ: Karpishin, T. B.; Stack, T. D. P.; Raymond, K. N. *J. Am. Chem. Soc.* **1993**, *115*, 182.

(59) SUCCUO: Stack, T. D. P.; Karpishin, T. B.; Raymond, K. N. *J. Am. Chem. Soc.* **1992**, *114*, 1512.

(60) FUDRUR: McMurphy, T. J.; Hosseini, M. W.; Garrett, T. M.; Hahn, F. E.; Reyes, Z. E.; Raymond, K. N. *J. Am. Chem. Soc.* **1987**, *109*, 7196.

(61) Hawkins, C. J. *Absolute Configuration of Metal Complexes, Inter-science Mono-graphs on Chemistry, Inorganic Chemistry Section*; Cotton, F. A., Wilkinson, G., Ed.; Wiley-Interscience: New York, 1971.

(62) Kepert, D. L. *Prog. Inorg. Chem.* **1977**, *23*, 1.



**Figure 5.** View down the  $C_3$  axis of the trigonal prismatic transition state for octahedral inversion in  $[\text{Ga}(\text{DIPTA})_3]^{3-}$  showing (a) steric congestion in the symmetrical structure and (b) how this congestion can be reduced by rotation of the  $N$ -isopropyl groups in one of the chelates.

for  $\text{Al}^{3+}$ .<sup>63</sup> Using a simple points-on-a-sphere repulsion model, Kepert showed that the barrier to octahedral inversion decreases as the normalized bite; in other words, the bite divided by the  $\text{M}-\text{O}$  distance, decreases.<sup>62</sup> Examination of tris-troponolate crystal structures<sup>63</sup> yields normalized bites of 1.36 for  $\text{Co}^{3+}$  and 1.32 for  $\text{Al}^{3+}$ . In  $[\text{Fe}(\text{CAT})_3]^{3-}$ , the normalized bite is 1.29 (see Table 5). Thus, the barriers for inversion follow the trend,  $\text{Co}^{3+} > \text{Al}^{3+} > \text{Fe}^{3+}$ , that is expected on the basis of the extent of  $\text{O}-\cdots\text{O}$  repulsion in the inner coordination sphere.

Barrier heights have been reported for intramolecular octahedral inversion in a tris-chelate complex involving catecholamide ligands. The  $\Delta H_{\text{inv}}^{\ddagger}$  values for  $[\text{Ga}(\text{DIPTA})_3]^{3-}$  range from 14 to 18 kcal/mol depending upon the solvent and the counterion.<sup>65</sup> This range is significantly higher than the  $\Delta E_{\text{inv}}$  calculated for  $[\text{Fe}(\text{CAT})_3]^{3-}$ . With a normalized bite of 1.31,<sup>58,66</sup> inner sphere repulsion in the  $\text{Ga}^{3+}$  complex should yield an inversion barrier between that of  $\text{Fe}^{3+}$  and  $\text{Al}^{3+}$ . For example, MM3 calculations on  $[\text{Ga}(\text{CAT})_3]^{3-}$  yield a  $\Delta E_{\text{inv}} = 8.4$  kcal/mol after modifying the parameter set for application to  $\text{Ga}^{3+}$  by adjusting one parameter, the  $\text{M}-\text{O}$  strain free length, from 1.931 to 1.860 Å to reproduce the experimental  $\text{Ga}-\text{O}$  distance of 1.96 Å.<sup>58,66</sup>

Further MM3 calculations on the  $[\text{Ga}(\text{DIPTA})_3]^{3-}$  complex reveal that the higher barrier derives from unfavorable steric interactions between the  $N$ -isopropyl substituents as shown in Figure 5. Concerted twisting of the chelates yields a trigonal prismatic structure with a  $C_3$  symmetry axis and a  $\Delta E_{\text{inv}}$  of 28.9 kcal/mol. In this structure (Figure 5a), dihedral angles about the  $\text{N}(\text{amide})-\text{C}(\text{isopropyl})$  bonds are distorted from the most stable rotamer in which the methyl groups straddle the  $\text{N}-\text{H}$  group. Steric strain in the trigonal prismatic structure can be lowered if the  $N$ -isopropyl groups in one of the chelates are rotated such that the methyl groups straddle the  $\text{C}=\text{O}$  group (Figure 5b). In this case  $\Delta E_{\text{inv}}$  drops to 19.5 kcal/mol, near the range of experimental values. Although other possible trigonal prismatic transition states remain to be examined, these results suggest that octahedral inversion in  $[\text{Ga}(\text{DIPTA})_3]^{3-}$  involves the concomitant rotation of at least one  $N$ -isopropyl group at

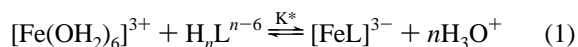
**Table 7.** Equilibrium Constants and  $\text{pFe}$  Values for Tris-Catecholamide Ligands<sup>a</sup>

ligand	$\Sigma \text{p}K_{\text{a}}$	$\log \beta_{116}$	$\log \beta_{110}$	$\text{pFe}^b$
$\text{H}_6\text{ENT}$	58.4	-9.7	48.7	35.6
$\text{H}_6\text{EMECAM}$	58.5	-11.4	47.1	32.6
$\text{H}_6\text{MMECAM}$	58.4	-12.6	45.8	31.2
$\text{H}_6\text{MECAM}$	58.0	-15.0	43.0	28.7
$\text{H}_7\text{TRENCAM}^+$	66.2	-2.6 <sup>c</sup>	43.6	27.8
$\text{H}_6,3,3,4\text{-CYCAM}$	62.1	-22.4	39.7	25.2

<sup>a</sup>  $\Sigma \text{p}K_{\text{a}}$  and  $\beta_{116}$  values are derived from experimental data<sup>27-30</sup> (see text).  $\log \beta_{110} = \log \beta_{116} + \Sigma \text{p}K_{\text{a}}$ . <sup>b</sup> Calculated under conditions of 1  $\mu\text{M}$   $[\text{Fe}]_{\text{total}}$ , 10  $\mu\text{M}$   $[\text{ligand}]_{\text{total}}$ , pH 7.4, and 25 °C. <sup>c</sup> Because  $\text{H}_7\text{TRENCAM}^+$  loses seven protons on  $\text{Fe}^{3+}$  complexation, this formation constant corresponds to the equilibrium  $[\text{FeL}_3^{3-}][\text{H}^+]^7/[\text{Fe}^{3+}][\text{H}_7\text{L}^+]$ .

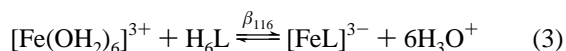
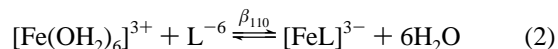
each cap of the trigonal prism to relieve steric congestion at the transition state.

**Structure/Function Correlations. (a) Thermodynamic Data.** Tris-catecholamide ligands form extremely stable complexes with  $\text{Fe}^{3+}$  making it impossible to use direct methods to measure the formation constants. However, proton-dependent formation constants,  $K^*$ , can be determined spectrophotometrically by competition with other ligands such as EDTA or DTPA.<sup>27-30</sup> These equilibria are expressed in terms of  $\text{H}_n\text{L}$  species (eq 1). If the ligand  $\text{p}K_{\text{a}}$ 's are known, then it is possible to derive formation constants for any protonation state of the ligand, including the fully deprotonated ligand.



The six catechol protons in these ligands fall into two groups, three acidic protons and three basic protons. In early assignments of tris-catecholamide formation constants, the acidic and basic  $\text{p}K_{\text{a}}$ 's in tris-catecholamides were assigned values of 8.4 and 12.1 based on measured values for a model compound, the secondary amide  $\text{H}_2\text{DMBA}$ .<sup>27</sup> Although it is not possible to determine the basic  $\text{p}K_{\text{a}}$ 's in tris-catecholamides, the acidic  $\text{p}K_{\text{a}}$ 's have been determined in subsequent studies. It was discovered that only  $\text{H}_6,3,3,4\text{-CYCAM}$ , which also contains secondary amide linkages, exhibited an average acidic  $\text{p}K_{\text{a}}$  similar to that of  $\text{H}_2\text{DMBA}$ .<sup>28</sup> The other tris-catecholamides,  $\text{H}_6\text{ENT}$ ,  $\text{H}_6\text{MECAM}$ ,  $\text{H}_6\text{MMECAM}$ ,  $\text{H}_6\text{EMECAM}$ , and  $\text{H}_7\text{TRENCAM}^+$ , which all contain primary amide linkages, exhibit acidic  $\text{p}K_{\text{a}}$ 's that are, on average, a log unit lower than that of  $\text{H}_2\text{DMBA}$ .<sup>29,30</sup>

With improved  $\text{p}K_{\text{a}}$  values, it is possible to update thermodynamic constants for the set of tris-catecholamides under consideration in this paper. The results are summarized in Table 7 which provides the sum of  $\text{p}K_{\text{a}}$ 's for each ligand, the log of the formation constant for the fully deprotonated form,  $\beta_{110}$  (eq 2), and the log of the formation constant for the fully protonated form,  $\beta_{116}$  (eq 3). Note that while the derivation of  $\beta_{110}$  values requires the assumption that the average basic  $\text{p}K_{\text{a}} = 12.1$  in all ligands, the  $\beta_{116}$  values are derived completely from measured experimental values. Table 7 also provides an updated set of  $\text{pFe}$  values, the negative logarithm of the free iron concentration under standard conditions of  $[\text{Fe}^{3+}]_{\text{total}} = 1 \mu\text{M}$  and  $[\text{ligand}]_{\text{total}} = 10 \mu\text{M}$  at pH 7.4 and 25 °C. These values were calculated using the program HySS<sup>67</sup> with iron hydrolysis included in the calculations.<sup>68</sup>



- (63) Eaton, S. S.; Hutchison, J. R.; Holm, R. H.; Muetterties, E. L. *J. Am. Chem. Soc.* **1972**, *94*, 6411. (b) Eaton, S. S.; Eaton, G. R.; Holm, R. H.; Muetterties, E. L. *J. Am. Chem. Soc.* **1973**, *95*, 1116.  
 (64) (a)  $[\text{Al}(\text{tropolonate})_3]$ : Muetterties, E. L.; Guggenberger, L. J. *J. Am. Chem. Soc.* **1972**, *94*, 8046. (b)  $[\text{Co}(\text{tropolonate})_3]$ : Doddrell, D. M.; Bendall, M. R.; Healy, P. C.; Smith, G.; Kennard, C. H. L.; Raston, C. L.; White, A. H. *Aust. J. Chem.* **1979**, *32*, 1219.  
 (65) Kersting, B.; Telford, J. R.; Meyer, M.; Raymond, K. N. *J. Am. Chem. Soc.* **1996**, *118*, 5712.  
 (66) Meyer, M.; Kersting, B.; Powers, R.; Raymond, K. N. *Inorg. Chem.* **1997**, *36*, 5179.



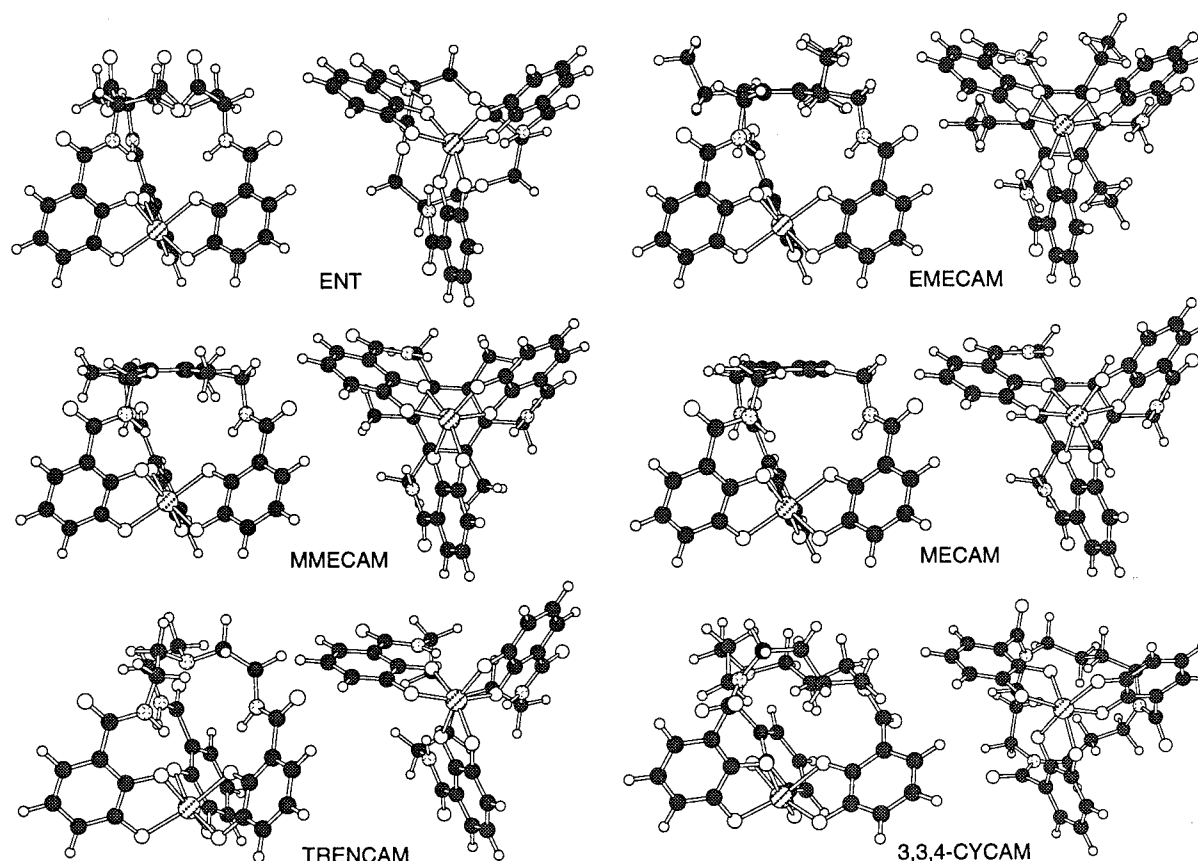


Figure 6. Lowest energy structures located by conformational searches on  $\text{Fe}^{3+}$  complexes.

**(b) Predicted Structures for the  $\text{Fe}^{3+}$  Complexes.** Conformer searches on the  $\text{Fe}^{3+}$  complexes with ENT, EMECAM, MMECAM, MECAM, TRENCAM, and 3,3,4-CYCAM were done to identify the most stable structures. We define stable structures as those within 4 kcal/mol of the minimum energy structure, in other words, to conformers that are  $\geq 0.1\%$  populated at room temperature. The stable conformers for each complex are discussed below. The population of each conformer, calculated at  $25^\circ$  from the relative steric energy, is given as a percentage in parentheses. The minimum energy structures for all the complexes are shown in Figure 6.

The  $\text{Fe}^{3+}$  complex of ENT exhibits two stable conformers. The lowest energy conformer has the  $\Delta$  configuration (97.0%) and the second conformer, 2.06 kcal/mol higher in energy, has the  $\Lambda$  configuration (3.0%). This result is consistent with experimental data. In the crystal structure of  $[\text{V}(\text{ENT})]^{2-}$ , the ligand adopts the same  $\Delta$  conformer<sup>69</sup> that is calculated for  $\text{Fe}^{3+}$  and CD spectra of  $[\text{Fe}(\text{ENT})]^{3+}$  and other ENT metal complexes reveal that the  $\Delta$  conformer predominates in solution.<sup>59,70</sup> The MM3 results are consistent with findings from prior modeling studies in which both a  $\Delta$  conformer and a higher energy  $\Lambda$  conformer are reported.<sup>69,71</sup> However, previous models find the

energy difference to be 0.5 kcal/mol (CFF force field)<sup>71</sup> and 6.93 kcal/mol (CACH force field).<sup>69</sup>

The  $\text{Fe}^{3+}$  complex of MECAM has only one conformer that exists as a mixture of two energetically degenerate  $\Delta$  and  $\Lambda$  stereoisomers (100%). MMECAM and EMECAM exhibit stable conformers that correspond to the MECAM structure. However, in these cases, rotation of the arene alkyl substituents gives rise to additional conformations. MMECAM has four stable conformers, each with  $\Delta$  and  $\Lambda$  configurations. In the lowest energy form (88.8%), the methyl groups are rotated such that the C—H groups eclipsing the arene all point toward carbonyl oxygens.  $60^\circ$  rotation of one, two, or all three of the methyl groups in MMECAM yields three additional sets of enantiomers at 1.36 (9.0%), 2.34 (1.7%), and 3.06 (0.5%) kcal/mol, respectively. EMECAM has three stable conformers, each with  $\Delta$  and  $\Lambda$  configurations. In the lowest energy conformer of EMECAM (93.6%), the ethyl substituents are oriented at  $\sim 90^\circ$  to the arene, and their methyl groups are on the side of the arene opposite to that of the metal ion.  $180^\circ$  rotation of one or two of the ethyl groups yields two pairs of stable conformers at 1.62 (6.1%) and 3.43 (0.3%) kcal/mol, respectively. A conformer with one rotated ethyl group has been observed in a crystal structure of the  $[\text{V}(\text{EMECAM})]^{2-}$  complex.<sup>29</sup>

The  $\text{Fe}^{3+}$  complex of TRENCAM has three stable conformers, all of which exist as pairs of energetically degenerate  $\Delta$  and  $\Lambda$  configurations. The lowest energy conformer (85.2%) and the two higher energy conformers at 1.38 (8.4%) and 1.53 (6.4%) kcal/mol are distinguished by the configuration of the triethylamine backbone. The highest energy of these three conformers is the conformer observed in  $[\text{Fe}(\text{TRENCAM})]^{3+}$  and  $[\text{V}(\text{TRENCAM})]^{3-}$  crystal structures.<sup>59,72</sup>

(67) Alderighi, L.; Gans, P.; Ineco, A.; Peters, D.; Sabatini, A.; Vacca, A. *Coord. Chem. Rev.* **1999**, *184*, 311.

(68) Baes, C. F.; Mesmer, R. E. *The Hydrolysis of Cations*; Wiley: New York, 1976.

(69) JOSLOS: Karpishin, T. B.; Dewey, T. M.; Raymond, K. N. *J. Am. Chem. Soc.* **1993**, *115*, 1842.

(70) (a) Isied, S. S.; Kuo, G.; Raymond, K. N. *J. Am. Chem. Soc.* **1976**, *98*, 1763. (b) McArdle, J. V.; Sofen, S. R.; Cooper, S. R.; Raymond, K. N. *Inorg. Chem.* **1978**, *17*, 3075.

(71) Shanzer, A.; Libman, J.; Lifson, S.; Felder, C. E. *J. Am. Chem. Soc.* **1986**, *108*, 7609.

**Table 8.** Calculated Structural Features of Lowest Energy Structures for Fe<sup>3+</sup> Tris-Catecholamides<sup>a</sup>

complex	Fe—O <sub>ortho</sub>	Fe—O <sub>meta</sub>	O—Fe—O	bite	O—O <sub>ortho</sub>	O—O <sub>meta</sub>	Fe—O—C	Fe—O—C—C	twist angle
ENT	2.016	2.022	80.4	2.608	2.705	2.886	112.6	4.3	34.7
EMECAM	2.025	2.024	80.2	2.607	2.819	2.870	112.9	3.4	38.8
MMECAM	2.021	2.021	80.4	2.608	2.800	2.911	112.7	4.9	41.2
MECAM	2.020	2.019	80.5	2.610	2.794	2.933	112.4	6.7	42.7
TRENCAM	2.015	2.019	80.4	2.604	2.676	3.032	111.4	12.3	43.1
3,3,4-CYCAM	2.022	2.035	79.2	2.584	2.764	3.211	111.7	13.3	52.1

<sup>a</sup> Units: Distances in Å, angles in degrees. See footnotes of Table 5 for definitions. Ortho and meta designations refer to the catecholate oxygen atom position with respect to the amide substituent.

The Fe<sup>3+</sup> complex of 3,3,4-CYCAM has three stable structures, but unlike MECAM, MMECAM, EMECAM, and TRENCAM, this asymmetric ligand does not exhibit energetically degenerate  $\Delta$  and  $\Lambda$  configurations. The lowest energy structure (73.0%) and the two higher energy structures at 0.63 (25.2%) and 2.18 (1.8%) kcal/mol are distinguished by the configuration of the macrocyclic. Each of these structures exhibits a different conformation of the 13-membered ring.

Structural features for the Fe(CAT)<sub>3</sub> component of the lowest energy conformers are summarized in Table 8. On comparing these data with the structural features of [Fe(CAT)<sub>3</sub>]<sup>3-</sup>, it is possible to draw some conclusions regarding the complementarity provided by the differing backbones. Although there is not much variation in Fe—O distances, O—Fe—O and Fe—O—C angles, and the bite, there are significant differences in the O—O distances in each cap of the pseudo-octahedra, the Fe—O—C—C dihedral angles, and the twist angles. Examination of the [Fe(CAT)<sub>3</sub>]<sup>3-</sup> structure, in which the three catechol groups are free to attain their optimal arrangement, suggests that the most complementary orientation of the catechol ligands is characterized by an O—O<sub>cap</sub> distance of 2.909 Å, Fe—O—C—C dihedral angles of 0°, and a twist angle of 48° (see Table 5). On comparison with the tris-catecholamide structural features (Table 8), it can be seen that none of the backbones provides the ideal orientation. In all of the tris-catecholamide structures, the O—O distance in the *ortho* cap is smaller than the ideal value and, in most cases, the O—O distance in the *meta* cap is larger than the ideal value. This indicates that the backbone constrains the catechol oxygen donors to lie on the surface of a cone rather than the preferred surface of a cylinder. The most severe distortions occur in TRENCAM and 3,3,4-CYCAM. All structures have nonzero Fe—O—C—C dihedral angles, again with TRENCAM and 3,3,4-CYCAM showing the largest distortions. Finally, the twist angles show significant deviation from 48° with the largest distortion occurring in ENT. These comparisons suggest that the ability of the ligand backbone to provide the optimal arrangement of catechol ligands decreases in the order EMECAM  $\approx$  MMECAM  $\approx$  MECAM  $>$  ENT  $>$  TRENCAM  $\approx$  3,3,4-CYCAM. As shown in the next section, this order is confirmed and quantified through analysis of strain energies.

**(c) Analysis of Structural Complementarity for Fe<sup>3+</sup>.** In the second paper of this series,<sup>22</sup> we presented a method for using MM calculations to quantitatively measure the ligand properties of complementarity and preorganization. In this approach, metal ion complementarity is measured by the change in ligand steric energy on going from the binding conformation of the ligand to the metal-bound form of the ligand. Thus, structural complementarity is measured by the amount of strain induced in the ligand upon metal ion complexation.

Application of this method requires the calculation of the structure of the ligand binding conformation in the absence of

the metal ion. When such calculations are done with charge-neutral ligands, it is assumed that the structures are representative of those that occur in condensed phases and, in the case of polyethers, this assumption is supported by numerous comparisons between calculated and observed structures.<sup>24,32,73–78</sup> When such calculations are done on charged ligands, such as the hexaanion produced by removal of Fe<sup>3+</sup> from a tris-catecholamide complex, it cannot be assumed that the isolated structure will resemble the structures found in condensed phases. Therefore, it is necessary to apply an alternate approach to evaluate the degree of complementarity in the tris-catecholamides.

Confronted with the same problem, Shanzer et al. developed a procedure to estimate the strain developed on Fe<sup>3+</sup> complexation in their prior MM analysis of ENT and MECAM.<sup>71</sup> This procedure involved cutting the complex into two pieces by breaking the C(amide)—N(amide) bonds. Further optimization on each piece allowed the calculation of the change in steric energy,  $\Delta U$ , on going from the initial state to the final equilibrium state. The changes in steric energy for each piece were added to give a measure of the strain originally present in the complex.

We adopted this approach to obtain a measure of the strain in the tris-catecholamide complexes. In this application, we separated the calculated structures of the complexes (Figure 6) into a backbone component and a tris-catecholate complex component by breaking the C(arene)—C(amide) bonds. Hydrogen atoms were added to the termini of the broken bonds at the ideal C—H distances and X—C—H angles (X = any atom). Each piece was optimized yielding a change in steric energy for the backbone,  $\Delta U_{\text{backbone}}$ , and the change in steric energy for the complex,  $\Delta U_{\text{complex}}$ . The sum of these strain energies provides a measure of the total strain energy in the original complex,  $\Delta U_{\text{total}}$ .

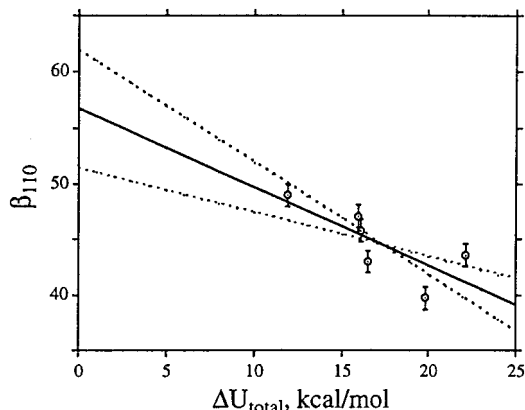
The results of this component analysis are presented in Table 9. Examination of the  $\Delta U_{\text{complex}}$  values confirms the ordering obtained through comparison of structural features in these complexes with those that occur in [Fe(CAT)<sub>3</sub>]<sup>3-</sup> (vide supra), that is, the strain in the tris-catecholate components increases in the order EMECAM  $<$  MMECAM  $<$  MECAM  $<$  ENT  $<$  TRENCAM  $<$  3,3,4-CYCAM. Thus, on examination of both structure and strain in the tris-catecholate component alone, one would conclude that EMECAM provides the most complementary binding site. It is necessary, however, to consider the total

(72) JEFZOJ: Bulls, A. R.; Pippin, C. G.; Hahn, F. E.; Raymond, K. N. *J. Am. Chem. Soc.* **1990**, *112*, 2627.

(73) Hay, B. P.; Rustad, J. R.; Zipperer, J. P.; Wester, D. W. *J. Mol. Struct. (THEOCHEM)* **1995**, *337*, 39.  
 (74) Paulsen, M. D.; Rustad, J. R.; Hay, B. P. *J. Mol. Struct. (THEOCHEM)* **1997**, *397*, 1.  
 (75) Hay, B. P.; Yang, L.; Zhang, D.; Rustad, J. R.; Wasserman, E. *J. Mol. Struct. (THEOCHEM)* **1997**, *417*, 19.  
 (76) Paulsen, M. D.; Hay, B. P. *J. Mol. Struct. (THEOCHEM)* **1998**, *429*, 49.  
 (77) Bryan, J. C.; Sachleben, R. A.; Lavis, J. M.; Burns, J. H.; Hay, B. P. *Inorg. Chem.* **1998**, *37*, 2749.  
 (78) Bryan, J. C.; Sachleben, R. A.; Hay, B. P. *Inorg. Chim. Acta* **1999**, *290*, 86.

**Table 9.** Steric Strains (kcal/mol) from Component Analysis

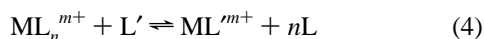
complex	$\Delta U_{\text{complex}}$	$\Delta U_{\text{backbone}}$	$\Delta U_{\text{total}}$
ENT	3.72	8.14	11.86
EMECAM	1.85	14.11	15.96
MMECAM	1.83	14.27	16.10
MECAM	2.13	14.34	16.47
TRENCAM	7.06	15.10	22.15
3,3,4-CYCAM	10.72	9.10	19.82

**Figure 7.** Plot of  $\log \beta_{110}$  versus  $\Delta U_{\text{total}}$ . Linear regression: slope =  $-0.705 \pm 0.304$ , intercept =  $56.7 \pm 5.3$ ,  $r = 0.758$ . Error bars show an uncertainty of  $\pm 1$  log unit.

strain in each complex to assess the impact of structure on binding affinity. When the  $\Delta U_{\text{backbone}}$  is added to  $\Delta U_{\text{complex}}$ , the total strain energies indicate that complementarity for  $\text{Fe}^{3+}$  decreases in the order  $\text{ENT} > \text{EMECAM} > \text{MMECAM} > \text{MECAM} > 3,3,4\text{-CYCAM} > \text{TRENCAM}$ . Thus, although ENT does not provide an optimal tris-catecholate geometry, the tris-catecholate geometry that it does provide is achieved with the least amount of strain in the backbone. In terms of  $\Delta U_{\text{total}}$ , we find ENT provides the most complementary binding site.

There is a rough correlation between the experimental  $\text{Fe}^{3+}$  binding affinity as measured by  $\beta_{110}$  (eq 2) and the degree of complementarity measured by  $\Delta U_{\text{total}}$ . A plot of  $\log \beta_{110}$  versus  $\Delta U_{\text{total}}$  shown in Figure 7 reveals the expected trend of increasing binding affinity with decreasing strain energy. We note that even the best ligand, ENT with a  $\log \beta_{110} = 48.7$ , contains a significant amount of strain energy, 11.86 kcal/mol. This result suggests that significantly higher  $\text{Fe}^{3+}$  binding affinities could be attained with more complementary architectures. On extrapolation to a  $\Delta U_{\text{total}}$  of zero, we estimate that a tris-catecholate ligand architecture with a perfect complementarity for  $\text{Fe}^{3+}$  would yield a  $\log \beta_{110} = 57 \pm 5$ , in other words, a  $\beta_{110}$  of  $8 \pm 5$  orders of magnitude larger than that exhibited by ENT.

This prediction is supported by an alternative estimate for the maximum value of  $\beta_{110}$  that can be obtained from the formation constant for  $[\text{Fe}(\text{DMBA})_3]^{3-}$ ,  $\log \beta_3 = 40.2$ ,<sup>27</sup> by considering the entropic consequences of connecting three DMBA ligands together. Consider eq 4 in which a metal complex undergoes a substitution reaction to



replace  $n$  ligands,  $\text{L}$ , with one ligand of equivalent denticity,  $\text{L}'$ . Assume that  $\Delta H = 0$ , in other words, that the free energy change for this reaction depends entirely upon  $\Delta S$ . The entropy for a mole of solute in aqueous solution at a standard state of 1 molal concentration in aqueous solution at 25 °C,  $S^0$ , is given by eq 5 where  $\text{Mw}$  is the molecular weight of the solute,  $V_m$  is

the molar volume of the pure liquid solute, and  $A$  and  $B$  are empirical constants with values of 10.0 cal/mol·K and 0.22 cal/cm<sup>3</sup>·K, respectively.<sup>79</sup>

$$S^0 = \frac{3}{2}R \ln(\text{Mw}) + S_{\text{int}} + A - BV_m \quad (5)$$

In a prior analysis of eq 4 where  $n = 2$ , Munro used eq 5 to derive an expression for  $\Delta S^0$  that depends only on the molecular weight of  $\text{L}$ .<sup>80</sup> In this derivation it is assumed that (i) the entropies of  $[\text{ML}_n]^{m+}$  and  $[\text{ML}']^{m+}$  are equivalent, (ii) the  $\text{Mw}$  of  $\text{L}'$  is approximately  $n$  times the  $\text{Mw}$  of  $\text{L}$ , and (iii) the molar volume of  $\text{L}'$  is approximately  $n$  times the molar volume of  $\text{L}$ . With the same approach, we derive the general expression in eq 6 where  $\Delta S^0$  is the entropy change in units of cal/mol·K for replacing  $n$  equivalent ligands with one multidentate ligand of the same denticity at a standard state of 1 molal in aqueous solution at 25 °C,  $\text{Mw}(\text{L})$  = molecular weight of  $\text{L}$ ,  $S_{\text{int}}(\text{L})$  is the internal entropy of  $\text{L}$  and  $S_{\text{int}}(\text{L}')$  is the internal entropy of  $\text{L}'$ . If we make the further assumptions that (iv)  $S_{\text{int}} = S_{\text{rot}} + S_{\text{vib}}$  and (v)  $S_{\text{vib}}(\text{L}')$  is approximately  $n$  times  $S_{\text{vib}}(\text{L})$ , then we arrive at eq 7. Assumption (v) will be the most valid when the backbone of the multidentate ligand is rigid, in other words, when the vibrational degrees of freedom in  $\text{L}'$ , which would correspond to the lost rotational and translation degrees of freedom in  $n\text{L}$ , are of high frequency.

$$\Delta S^0 = \frac{3}{2}R \ln \left[ \frac{\text{Mw}(\text{L})^{n-1}}{n} \right] + (n-1) 10.0 + nS_{\text{int}}(\text{L}) - S_{\text{int}}(\text{L}') \quad (6)$$

$$\Delta S^0 = \frac{3}{2}R \ln \left[ \frac{\text{Mw}(\text{L})^{n-1}}{n} \right] + (n-1) 10.0 + nS_{\text{rot}}(\text{L}) - S_{\text{rot}}(\text{L}') \quad (7)$$

Rotational entropies were obtained from MM3 calculations which gave  $S_{\text{rot}} = 31.1$  cal/mol·K for DMBA and  $S_{\text{rot}}$  values in the range of  $37.7 \pm 0.5$  cal/mol·K for the protonated tris-catecholate ligands examined in this study (vide infra). Application of eq 6 to DMBA ( $\text{Mw}(\text{L}) = 181.08$  g/mol,  $n = 3$ ,  $S_{\text{rot}}(\text{L}) = 31.1$  cal/mol·K,  $S_{\text{rot}}(\text{L}') = 37.7$  cal/mol·K) yields  $\Delta S^0 = 104.5$  cal/mol·K. At 25 °C, this corresponds to a free energy change of  $-31.1$  kcal/mol or an increase of  $10^{22.8}$  in the formation constant for  $[\text{Fe}(\text{DMBA})_3]^{3-}$ . Combining this result with the  $\log \beta_3$  of 40.2, we estimate that  $\log \beta_{110} = 63.0$  if the entropic cost of assembling the three DMBA ligands was paid prior to  $\text{Fe}^{3+}$  complexation. This estimate only slightly exceeds the high end of the  $57 \pm 5$  range extrapolated from the  $\log \beta_{110}$  versus  $\Delta U_{\text{total}}$  plot (Figure 7).

**(d) Theoretical Relationship between Binding Constants and Strain Energies.** In the preceding section, we found  $\log \beta_{110}$  to be roughly correlated with the strain in the metal complex, in other words, with an energetic quantity that measures  $\text{Fe}^{3+}$  complementarity. This analysis ignores a component of the overall strain present in the system, that is, the strain associated with the conformational reorganization of the ligand. When the uncomplexed ligand conformer differs from the binding conformer, then it is also necessary to consider the energy difference between the two ligand conformers. It is difficult to evaluate this quantity for the reaction shown in eq 2 because, as discussed above, this would entail the conformational analysis of isolated hexa-anionic ligands leading to

(79) Powell, R. E.; Latimer, W. M. *J. Chem. Phys.* **1951**, *19*, 1139.(80) Munro, D. *Chem. Br.* **1977**, *13*, 100.



**Table 10.** Hydrogen Bond Distances (Å) in Protonated Ligands<sup>a</sup>

	O—H ··· O=C	intrachelate O—H ··· O—H	interchelate O—H ··· O—H	N—H ··· O—H	N—H ··· O(ester)
H <sub>6</sub> ENT, 1		2.16, 2.18, 2.34	1.99, 2.07, 2.15, 2.15, 2.19	1.92, 1.93, 1.94	2.24, 2.28
H <sub>6</sub> ENT, 2	1.80, 1.80, 1.80	2.18, 2.18, 2.18			2.20, 2.20, 2.20
H <sub>6</sub> ENT, 3	1.81, 1.81, 1.81	2.19, 2.19, 2.19			2.34, 2.34, 2.34
H <sub>6</sub> MECAM, 1	1.81, 1.82, 1.83	2.18, 2.21, 2.22	1.99, 2.01, 2.06, 2.08		
H <sub>6</sub> MECAM, 2	1.80, 1.83	2.16, 2.29, 2.34	1.94, 1.99, 2.00, 2.03, 2.05	2.07	
H <sub>6</sub> 3,3,4-CYCAM	1.85, 1.85, 1.87	2.19, 2.21, 2.22	2.00, 2.13		

<sup>a</sup> H ··· O distances (Å) less than 2.4 Å for structures shown in Figure 8.

unrealistic, high energy structures for comparison with condensed phase. An alternative is to perform the strain energy analyses for the reaction shown in eq 3 where the complexation is defined in terms of fully protonated, neutral ligands. The following arguments show how it is possible to relate  $\beta_{116}$  to the steric energies of the  $[\text{FeL}]^{3-}$  complex and the protonated ligand, H<sub>6</sub>L.

The free energy for the reaction in eq 3 can be expressed as the difference in free energies between the products and reactants (eq 8). Realizing that the quantity  $[6G^0(\text{H}_3\text{O}^+) - G^0(\text{Fe}(\text{OH})_2^{3+})]$  is a constant, we can write eq 9. The enthalpy difference in eq 9 can be defined as the sum of two quantities,  $\Delta U^*$  and  $\Delta H_{\text{int}}^0$  (eq 10), where  $\Delta U^* = U(\text{FeL}^{3-}) - U(\text{H}_6\text{L})$  and  $\Delta H_{\text{int}}^0$  is the intrinsic enthalpy difference between 6 H—O ionic bonds and 6 Fe—O ionic bonds. If we assume that  $\Delta H_{\text{int}}^0$  is constant, then differences in enthalpy are due entirely to differences in  $\Delta U^*$ . In practice,  $\Delta U^*$  is defined as the difference in steric energy between the lowest energy form of the complex and the lowest energy form of the ligand.

$$\Delta G_{116}^0 = G^0(\text{FeL}^{3-}) + 6 G^0(\text{H}_3\text{O}^+) - G^0(\text{H}_6\text{L}) - G^0(\text{Fe}(\text{OH})_2^{3+}) \quad (8)$$

$$\Delta G_{116}^0 = H^0(\text{FeL}^{3-}) - H^0(\text{H}_6\text{L}) - T[S^0(\text{FeL}^{3-}) - S^0(\text{H}_6\text{L})] + c_1 \quad (9)$$

$$H^0(\text{FeL}^{3-}) - H^0(\text{H}_6\text{L}) = \Delta U^* + \Delta H_{\text{int}}^0 = \Delta U^* + c_2 \quad (10)$$

To obtain a linear relationship between  $\Delta G_{116}^0$  and  $\Delta U^*$ , the entropy difference in eq 9 is either (i) constant or (ii) proportional to the enthalpy difference (eq 11). The second possibility is supported by the fact that linear dependencies between  $\Delta H$  and  $\Delta S$  have been observed for many reaction series.<sup>81</sup> Substitution of eq 10 and 11 into eq 9 yields eq 12 which may also be written as eq 13. If case (i) applies, then plots of  $\Delta G_{116}^0$  and  $\log \beta_{116}$  versus  $\Delta U^*$  should exhibit slopes of 1.00 and,  $-0.733$  at 25 °C, respectively. If case (ii) applies, then the slopes would be expected to deviate from these values.

$$-T[S^0(\text{FeL}^{3-}) - S^0(\text{H}_6\text{L})] = c_3[H^0(\text{FeL}^{3-}) - H^0(\text{H}_6\text{L})] + c_4 \quad (11)$$

$$\Delta G_{116}^0 = c_5 \Delta U^* + c_6 \quad (12)$$

$$\log \beta_{116} = \frac{-1}{2.303RT} [c_5 \Delta U^* + c_6] \quad (13)$$

**(e) Predicted Structures for Protonated Ligands.** Application of eq 13 to the series of tris-catecholamide ligands requires the evaluation of  $\Delta U^*$ . This evaluation requires the identification

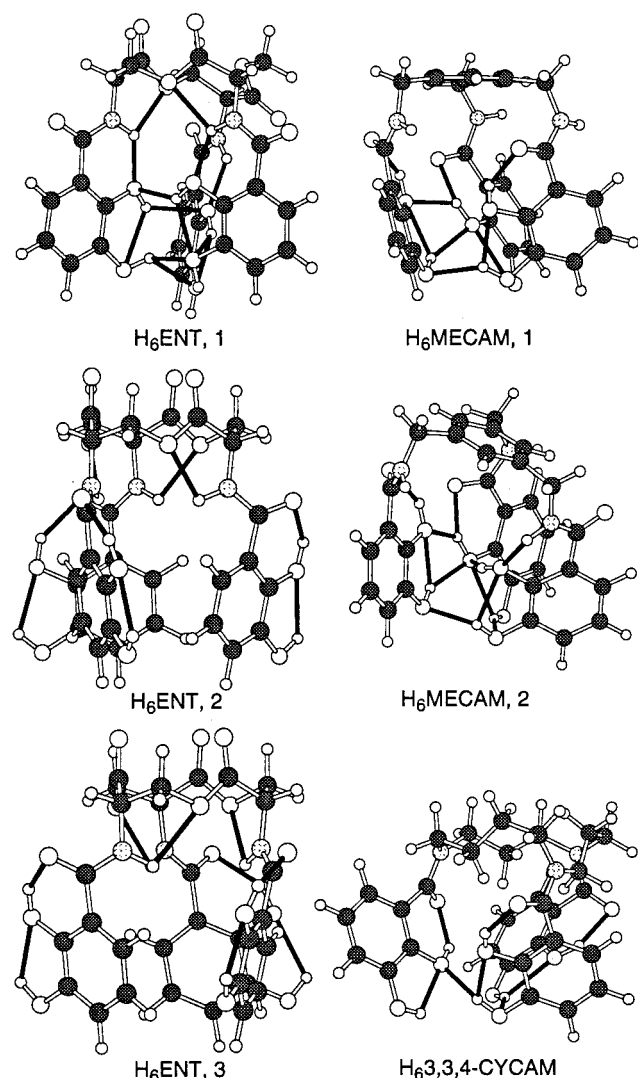
of the minimum energy conformations for the  $\text{Fe}^{3+}$  complexes (see Figure 6), and for the protonated ligands. In this section we summarize the results of conformer searches that were done on H<sub>6</sub>ENT, H<sub>6</sub>MECAM, H<sub>6</sub>MMECAM, H<sub>6</sub>MECAM, and H<sub>6</sub>3,3,4-CYCAM. Because  $\text{Fe}^{3+}$  complexation by H<sub>7</sub>TRENCAM<sup>+</sup> involves the loss of 7, rather than 6 protons, the reaction in eq 3 does not apply and H<sub>7</sub>TRENCAM<sup>+</sup> could not be included in this ligand series. As with the  $\text{Fe}^{3+}$  complexes, we define stable structures as those within 4 kcal/mol of the minimum energy structure and conformer populations, calculated at 25° from the relative steric energies, are given as percentages in parentheses. The stable conformers of the protonated ligands are characterized by the presence of extensive intramolecular hydrogen bonding. Table 10 lists all O—H ··· O and N—H ··· O hydrogen bond distances  $\leq 2.40$  Å for each of the low energy structures shown in Figure 8.

H<sub>6</sub>ENT exhibits five stable conformers. The three lowest energy structures are shown in Figure 9. In the lowest energy conformer (78.6%), the macrocyclic ring adopts a high energy configuration in which one of the carbonyl groups is bent down toward the catecholamide groups. In addition, each of the catecholamide groups exhibit the less stable hydrogen bonding motif (Figure 2b). The destabilization associated with these structural features is compensated for by the presence of six inter-chelate O—H ··· OH hydrogen bonds. The second and third conformers at 0.88 (17.8%) and 1.88 (3.3%) kcal/mol both exhibit the low energy macrocycle conformation and each of the catecholamide groups exhibit the more stable hydrogen bonding motif (Figure 2a). However, these two structures do not have any inter-chelate O—H ··· OH hydrogen bonds. These two conformers, which both have a C<sub>3</sub> symmetry axis, are distinguished by the N—H ··· O(ester) hydrogen bonds. These hydrogen bonds form five-membered rings involving N—CH(R)—C(=O)—O in the second conformer and N—CH(R)—CH<sub>2</sub>—O in the third conformer. The fourth and fifth conformers at 3.43 (0.24%) and 3.71 (0.16%) kcal/mol are variants of the lowest energy conformer.

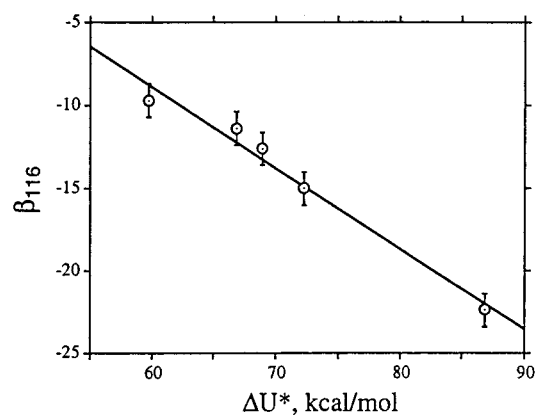
H<sub>6</sub>MECAM exhibits the two stable conformers shown in Figure 8. In the lowest energy conformer (83.2%) all of the catecholamide groups adopt the more stable hydrogen bonding motif (Figure 2a) and there are four interchelate O—H ··· O—H hydrogen bonds. In the second conformer, at 0.95 (16.7%) kcal/mol, one of the catecholamide groups adopts the less stable hydrogen bonding motif (Figure 2b) to allow the formation of five interchelate O—H ··· O—H hydrogen bonds. As in the conformational analysis of the  $\text{Fe}^{3+}$  complexes, H<sub>6</sub>MMECAM and H<sub>6</sub>MECAM exhibit analogous behavior to H<sub>6</sub>MECAM. In both cases, populated conformers (>99%) exhibit the hydrogen bonding of the two low energy H<sub>6</sub>MECAM conformers. These conformer populations consist of a dominant form and minor forms deriving from rotation of the arene alkyl substituents.

H<sub>6</sub>3,3,4-CYCAM exhibits five stable conformers with the lowest energy conformer shown in Figure 8. The lowest energy

(81) (a) Leffler, J. E. *J. Org. Chem.* **1955**, *20*, 1202. (b) Leffler, J. E.; Grunwald, E. *Rates and Equilibria of Organic Reactions*; John Wiley and Sons: New York, 1963; Chapter 9. (c) Grunwald, E.; Steel, C. J. *Am. Chem. Soc.* **1995**, *117*, 5687.



**Figure 8.** Lowest energy structures for protonated ligands. Hydrogen bonds are indicated with solid black lines.



**Figure 9.** Plot of  $\log \beta_{116}$  versus  $\Delta U^*$ . Linear regression: slope =  $-0.49 \pm 0.04$ , intercept =  $20.7 \pm 3.1$ ,  $r = 0.988$ . Error bars show an uncertainty of  $\pm 1$  log unit.

conformer (96.8%) and the other conformers at 2.27 (2.0%), 3.03 (0.6%), 3.45 (0.3%), and 3.63 (0.2%) kcal/mol differ in the number of interchelate hydrogen bonds and the conformation of the macrocyclic ring.

We note that the conformers calculated in this study correspond to the lowest energy forms in the gas phase. Hydrogen

bonding with solvent molecules will compete with intramolecular hydrogen bonding, and it is not clear to what extent these conformers will be populated in aqueous solution. With this in mind, we make the following “gas phase” observations. Examination of the low energy conformers of the neutral tris-catecholamide ligands confirms that major structural reorganization occurs on going from the protonated form to the  $\text{Fe}^{3+}$  complex. The energetic cost of this reorganization will increase as the extent of intramolecular hydrogen bonding increases, in other words, as the protonated ligand becomes more stable. The O—H...O=C interactions are the strongest hydrogen bonds that can form in these structures. However, the results on  $\text{H}_6\text{ENT}$  and  $\text{H}_6\text{MECAM}$  reveal that loss of one or more of these hydrogen bonds allows the formation of low energy conformers characterized by extensive interchelate O—H...O—H interactions. A unique property of the ENT backbone is that it does not allow both types of interaction to occur simultaneously, thereby preventing additional stabilization of the uncomplexed ligand. In contrast, the other tris-catecholamide backbones yield structures that are stabilized by both O—H...O=C and interchelate O—H...O—H hydrogen bonding.

**(f) Quantitative Structure–Stability Relationship.** Subtracting the steric energy of the most stable  $\text{Fe}^{3+}$  complex from the steric energy of the most stable protonated ligand yields the following  $\Delta U^*$  values (kcal/mol): ENT, 59.74; EMECAM, 66.83; MMECAM, 68.93; MECAM, 73.27; and 3,3,4-CYCAM, 86.69. A plot of  $\log \beta_{116}$  versus  $\Delta U^*$  yields the linear correlation shown in Figure 9. The line passes through all points within  $\pm 1$  log unit. The slope of this plot,  $-0.490$ , deviates from the value expected for a constant entropy difference,  $-0.733$ , consistent with the presence of some enthalpy–entropy compensation, in other words, eq 10 applies to the reaction in eq 3 (vide supra).

Given the correlation shown in Figure 9, we find that the  $\Delta U^*$  values calculated from gas-phase structures provide an accurate predictive tool for how ligand architecture influences metal binding affinity. The correlation obtained on consideration of the strain within the metal complex alone (Figure 7) is improved by evaluating the total difference in steric energy between the protonated form and the metal complex, in other words, by including the energetic cost of conformational reorganization. The result provides a further demonstration of the utility of molecular mechanics analysis of isolated ligand structures to rationalize the influence of structure on binding affinity.

**Structural Design Criteria.** The structural design of ligands with high binding affinities involves the identification of backbones that provide complementary arrays of donor groups.<sup>1,9</sup> Useful design criteria include both a knowledge of optimal geometry and the energetic costs of failing to achieve various aspects of this geometry. The optimal geometry for placing three catecholate donor groups about  $\text{Fe}^{3+}$  is observed in the  $[\text{Fe}(\text{CAT})_3]^{3-}$  complex. Key features of this geometry include Fe—O distances of 2.17 Å, Fe—O—C—C dihedral angles of  $0^\circ$ , O—...O<sub>cap</sub> distances of 2.909 Å, and a twist angle of  $48^\circ$  (Table 6).

Failure to provide any one of these geometric features will lead to a loss of complementarity and result in destabilization of the complex. This is illustrated in Table 11 where we give the magnitude of selected structural distortions that is needed to destabilize the complex by 1, 2, and 3 kcal/mol. These distortions involve compressing or stretching all six Fe—O bonds, decreasing or increasing the three O—...O distances in one cap of the octahedron, distortion of Fe—O—C—C dihedral

**Table 11.** Energetic Penalties for Selected Distortions to the  $[\text{Fe}(\text{CAT})_3]^{3-}$  Structure<sup>a</sup>

	0 kcal/mol	1 kcal/mol	2 kcal/mol	3 kcal/mol
Fe—O compress	2.017	1.985	1.971	1.962
Fe—O stretch	2.017	2.055	2.070	2.085
decrease O—O—O <sub>cap</sub>	2.909	2.756	2.696	2.652
increase O—O—O <sub>cap</sub>	2.909	3.076	3.144	3.198
Fe—O—C—C dihedral	0.0	±7.8	±11.4	±14.0
decrease twist angle	48.0	40.9	37.2	33.5
increase twist angle	48.0	53.1	54.7	55.7

<sup>a</sup> Units: Distances in Å, angles in degrees.

angles to move all three catecholate groups out-of-plane with respect to the metal, and decreasing or increasing the twist angle.

The steric strain in the  $\text{Fe}(\text{CAT})_3$  components of ENT, EMECAM, MMECAM, MECAM, 3,3,4-CYCAM, and TREN-CAM ranges from 1.8 to 10.7 kcal/mol (Table 9). Comparison of the structural features in these complexes (Table 8) with the values in Table 11 reveals that in no case does significant destabilization arise from a failure of the backbone to accommodate Fe—O distance requirements. On the other hand, the structural constraints imposed by the different backbones do force energetically significant deviations to the inner-coordination sphere, as seen in the O—O—O<sub>cap</sub> distances and twist angles, and the orientation of the catecholate binding sites, as seen in the Fe—O—C—C dihedral angles. The data provided in Table 11 can be used to estimate the cost of these structural deviations. For example, the 3.7 kcal/mol of strain calculated for the  $\text{Fe}(\text{CAT})_3$  component of ENT derives primarily from the decreased twist angle, ~3 kcal/mol, and the decreased O—O—O<sub>cap</sub> distance, ~1 kcal/mol.

## Summary

We have presented the development of an MM3 model for catecholamides and their  $\text{Fe}^{3+}$  complexes. This model, based in part on fitting to geometries and energies from electronic structure calculations and in part on fitting to crystal structure data, is validated by its ability to reproduce experimental structure and barriers to octahedral inversion in tris-chelate

complexes. Application of this model yields the first quantitative structure—stability relationship for  $\text{Fe}^{3+}$  complexation by tris-catecholamides.

An evaluation of the degree of binding site organization in tris-catecholamides reveals that none of the backbones examined in this study provide architectures with optimum complementarity for  $\text{Fe}^{3+}$ . From a plot of  $\log \beta_{110}$  versus  $\Delta U_{\text{total}}$  and an evaluation of the entropy associated with connecting three DMBA chelates, we predict that increased complementarity in these ligands would yield significant,  $8 \pm 5$  orders of magnitude, increases in  $\text{Fe}^{3+}$  binding constant. This study has produced the tools needed to screen potential backbone structures to obtain more effective tris-catecholate siderophores, that is, structural criteria for evaluating the degree of binding site organization and methods for predicting the influence of ligand architecture on  $\text{Fe}^{3+}$  binding affinity.

**Acknowledgment.** This paper was supported in part under grant No. 64947, Environmental Management Science Program, Office of Science and Technology, Office of Environmental Management U. S. Department of Energy (DOE). Financial support for R. V. and J. G. was partially provided by CONACYT, México. This research was performed in part using the Molecular Science Computing Facility (MSCF) in the William R. Wiley Environmental Laboratory at the Pacific Northwest National Laboratory (PNNL). The MSCF is funded by the Office of Biological and Environmental Research in the U. S. Department of Energy. PNNL is operated by Battelle for the U. S. Department of Energy under contract DE-AC06-76RLO 1830.

**Supporting Information Available:** MM3 parameter files, MM3 input files for minimum energy structures of each ligand and  $\text{Fe}^{3+}$  complex, Cartesian coordinates of structures optimized with electronic structure calculations, table of observed and calculated structural features for chelated 2,3-dioxy-*N*-alkylbenzamide and 2,3-dihydroxy-*N*-alkylbenzamide, and potential energy surfaces for distortion of Fe—O distance and Fe—O—C—C in  $[\text{Fe}(\text{CAT})_3]^{3-}$ . This material is available free of charge via the Internet at <http://pubs.acs.org>.

IC001380S